Citation: Jian-Xin Lu, Peiliang Shen, Hafiz Asad Ali, Chi Sun Poon*, Development of high performance lightweight concrete using ultra high performance cementitious composite and different lightweight aggregates, Cement and Concrete Composites 124 (2021) 104277. https://doi.org/10.1016/j.cemconcomp.2021.104277

Development of high performance lightweight concrete using ultra high performance cementitious composite and different lightweight aggregates

Jian-Xin Lu, Peiliang Shen, Hafiz Asad Ali, Chi Sun Poon*

Department of Civil and Environmental Engineering,

The Hong Kong Polytechnic University, Hung Hom, Kowloon, Hong Kong, China

*Corresponding author: cecspoon@polyu.edu.hk

Abstract: To reduce the dead load of concrete structures, this study developed a high performance lightweight aggregate concrete (HPLAC) by combining the use of ultra high performance cementitious composite (UHPC) and different types of aluminosilicate lightweight aggregates (LWAs). The physicochemical properties of two types of LWAs (i.e. expanded clay and expanded shale) influencing the HPLAC were elaborated and compared. The composition distribution and micromechanical properties in the interfacial regions of paste and LWAs were revealed by elemental mapping and nanoindentation. The results showed that the incorporation of the clay LWAs or shale LWAs in the HPLAC led to similar density and thermal conductivity values, while the use of the shale LWAs induced a lower water absorption and higher strength of HPLAC as compared to the clay LWAs due to the fine pore structure and higher pozzolanic activity of the former. The internal curing effect provided by the pre-wetted shale LWAs was more efficient in enhancing the hydration of binder, and the Al dissolution from the shale LWAs further densified the interfacial bonding to form a dense rim surrounding LWAs, resulting in improved micromechanical properties at the interface. The X-ray CT results indicated that the adoption of UHPC was beneficial to preventing segregation of the LWAs and steel fibers in the HPLAC. By virtue of the physical-chemical interactions of LWAs, the synergetic use of UHPC and pre-wetted shale LWAs was able to produce an HPLAC with high structural efficiency, good thermal

insulation, low autogenous shrinkage and permeability.

Keywords: High performance lightweight concrete; Ultra high performance cementitious composite; Durability; Pozzolanic reactivity; Micromechanical properties

1 Introduction

Modular integrated construction (MiC) is perceived as an innovative construction concept by adopting two construction phases: factory assembly and on-site installation [1]. The development of the MiC in recent years seems to provide a solution for addressing the shortage of manpower, increased costs of construction, and declining productivity in the construction industry. Furthermore, the adoption of the MiC can increase the quality of construction, enhance site safety and reduce environmental impacts, thus the MiC is getting more popular around the world [2, 3]. However, conventional concrete materials similar to those used for on-site construction are normally used in the MiC [4], which poses challenges for requiring stronger hoist cranes and special logistics. Therefore, it is of significance to develop a high performance lightweight concrete for enhancing the lifting capacity and reducing the transportation cost of the MiC construction.

Lightweight aggregates (LWAs) are generally used to produce high strength lightweight concrete for structural applications. Due to the presence of pores in the LWAs, the weight of high-strength lightweight aggregate concrete (HSLAC) is 20~40% lower than conventional concrete, with density values of less than 2000 kg/m^3 [5] and 28 day compressive strength higher than 40 MPa [6]. To prepare high performance HSLAC, three strategies have been used: use of good-quality binder matrix, selection of proper LWAs, and addition of fibers.

For improving the quality of the binder matrix, supplementary cementitious materials (SCMs) and a low water-to-binder (w/b) ratio were adopted [7, 8]. Some researchers [9, 10] prepared HSLAC with the incorporation of silica fume, and found that the HSLAC had similar resistance to the chloride ion penetration and bond strength as compared to normal weight concrete. These findings are in agreement with the studies of Thomas and co-workers [11, 12], which indicated that the additions of SCMs (e.g. silica fume, fly ash, and blast furnace slag) were effective in decreasing

penetration of chloride ions in 25-year-old lightweight concrete compared to concrete containing only Portland cement. Nadesan and Dinakar [13] utilized silica fume and metakaolin to improve the mechanical and durability properties of HSLAC, and the benefits were more pronounced at a lower *w*/*b* ratio of 0.25. The study of Chen and Liu [14] indicated that the combined use of fly ash, blast furnace slag, and silica fume in HSLAC could prevent bleeding and up-floating of LWAs. To reduce the dead weight and increase the strength, Kılıç et al. [15] developed an HSLAC incorporating silica fume and fly ash. Similarly, Wilson and Malhotra [16] found that HSLAC prepared with silica fume had a satisfactory resistance to cyclic freezing and thawing. In addition, Seabrook and Wilson [17] pointed out that the optimum silica fume content was in the range of 5% to 10% by the weight of cement. Atmaca et al. [18] added 3% nano-silica into HSLAC to mitigate the negative effects of LWAs. As a result, a remarkable increase in mechanical properties and reductions in sorptivity and gas permeability were achieved. Except using the SCMs, by reducing the *w*/*b* ratio, Moreno et al. [19] prepared a more durable HSLAC (higher strength and lower ion permeability) in comparison to normal lightweight aggregate concrete with a higher *w*/*b* ratio. Real and his colleagues [20, 21] also reported that the dense HSLAC with lower *w*/*b* ratio had lower permeability regardless of the type of LWAs.

For producing high strength lightweight concrete, the type of LWAs used also plays a vital role. Several kinds of LWAs have been adopted in the production of HSLAC, including cold bonded and sintered fly ash LWAs [13, 18, 22, 23], expanded clay and slate [24-27], oil-palm-boiler clinker and oil palm shell [28-30], and other LWAs (e.g. scoria, tuff, expanded shale) [12, 15, 16, 31]. Kockal and Ozturan [23] produced a high strength sintered fly ash LWA (crushing strength of 12 MPa) and compared it with cold bonded sintered fly ash LWA (crushing strength of 3.7 MPa) in HSLAC. Their study showed that the HSLAC incorporating high strength LWAs had better mechanical properties (compressive and splitting tensile strengths, modulus of elasticity) than the HSLAC using low strength LWAs. In terms of durability performance, Real and Bogas [20] found that the permeability of HSLAC decreased when the open porosity of LWAs was reduced and the permeability of HSLAC with denser aggregates could be similar to that of normal weight concrete. They also reported a higher carbonation resistance of HSLAC prepared with the lower porosity LWAs [32]. Normally, the use of fine LWAs induced a higher compressive strength of lightweight concrete as compared to coarse LWAs [33, 34]. Moreover, the larger amount of fine LWAs could attain a higher compressive strength of HSLAC [35]. Due to the presence of lower stiffness of

LWAs, lightweight concrete usually exhibits lower flexural/tensile properties [36, 37] and higher long-term shrinkage [38]. Polypropylene and steel fibers have thus been added to enhance the flexural toughness and splitting tensile strength of HSLAC [39-42]. Compared to the polypropylene fibers, the addition of steel fibers was more effective in increasing the flexural strength and toughness [39, 42], whereas the latter increased the density considerably and reduce the slump of concrete [40, 41]. Thus, a proper volume fraction of steel fibers should be taken into account in the design of HSLAC. Since the LWAs have a lower modulus than the natural aggregates, other advantages of using fibers in HSLAC include the increase of modulus of elasticity [41], enhancement of ductility [42], and reduction of shrinkage [43] thanks to the crack arresting ability of the fibers.

Given the LWAs are the weakest component in the HSLAC, the durability and mechanical properties of the lightweight concrete would be mainly governed by the qualities of cement mortar forming a protective coating around the LWAs [44, 45]. Thus, how to improve the quality of the mortar matrix is the key point in the production of HSLAC. In this study, an ultra high performance cementitious composite (UHPC) was used as a binder to prepare the HSLAC to leverage its very high strength and superior durability. Previously, some studies [46-50] have incorporated pre-wetted LWAs into the low *w*/*b* concrete, but the intentions of these investigations were to enhance the strength [46, 49] or reduce the shrinkage [47, 48, 50] of high performance concrete, the weight of concrete was thus not reduced significantly (e.g. the density of the LWC was about 2,300 kg/m^3 in ref [46]). Therefore, this study aimed to produce high quality lightweight concrete combining 1) UHPC as a paste, and 2) a large volume of LWAs aiming to improve the performance of lightweight concrete and reduce the dead load of concrete.

Aforementioned, with the use of SCMs, good quality LWAs and fibers, the mechanical properties and durability of lightweight concrete can be enhanced considerably. Until now, few studies have provided a comprehensive perspective (i.e. an integration of the above three approaches) to produce a high-performance lightweight concrete. This work integrated the use of a UHPC paste, steel fibers and two typical types of LWAs (expanded clay and expanded shale) to produce a UHPC-based HPLAC. In particular, the roles of the physicochemical properties of LWAs in the UHPC matrix were emphatically investigated and compared.

2 Materials and methods

2.1 Materials

A Type I ordinary Portland cement (OPC) sourced from Hong Kong Green Island Cement Company was used as the main cementitious material. Silica fume (SF) and ground granulated blast furnace slag (GGBS) were purchased from Mainland China. Metakaolin (MK) was supplied by a local company (Nano and Advanced Materials Institute). The chemical compositions of the cementitious materials were analyzed by X-ray fluorescence technique using a Rigaku Supermini200 spectrometer. Table 1 lists the composition results, which show that the SF was rich in SiO_2, the MK was rich in SiO_2 and Al_2O_3, and the GGBS was rich in SiO_2 and CaO. The particle size distributions of cementitious materials (except SF) were measured by a laser diffraction analyzer (Malvern Instrument), while the size of SF was tested by a Zetasizer (Malvern, Nano-ZS90) due to its extremely fine particle. The particle size distributions are depicted in Fig. 1 and the average size and density of cementitious materials are shown in Table 1.

Table 1. Chemical compositions and physical properties of cementitious materials and aggregates.

Compositions (wt. %)	OPC	SF	MK	GGBS	CLWA	SLWA	RS
SiO_2	19.0	95.7	53.00	34.78	60.4	62.0	90.4
Al_2O_3	5.68	0.45	43.60	14.22	19.8	19.8	4.71
CaO	65.8	0.73	0.12	38.38	2.57	0.76	0.66
MgO	0.97	0.71	0.10	7.32	1.23	/	0.26
K_2O	0.66	1.74	1.68	0.77	2.89	4.58	2.06
P_2O_5	0.16	0.09	0.13	/	0.37	0.23	0.14
Fe_2O_3	3.12	0.07	0.70	0.27	11.2	7.16	0.88
Na_2O	/	/	/	/	/	1.29	0.66
SO_3	4.03	0.27	0.23	3.12	0.15	0.13	0.10
Physical properties							
Specific gravity	3.15	2.69	2.11	2.56	2.63	2.52	2.53
Average particle size (μm)	22.68	0.44	6.21	15.64	/	/	/

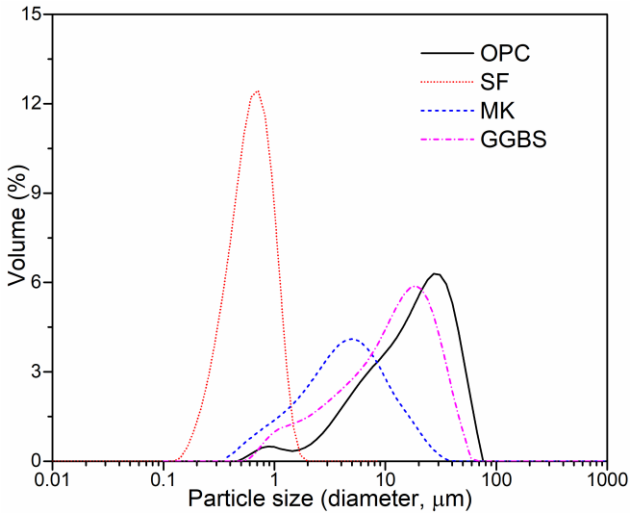

Fig. 1. Particle size distributions of cementitious materials.

Aggregates used in this study included river sand (RS), expanded clay lightweight aggregate (CLWA), and expanded shale lightweight aggregate (SLWA). The CLWA was made from fresh clay, and produced through pelletization and sintering in the form of rounded pellets. The angular shaped SLWA was crushed from a big bulk of expanded shale. Thus, the surface of the SLWA was very rugged and the surface pores were open (see Fig. 2). The particle size of these aggregates was ranged between 2.36-5 mm as finer LWAs usually have a higher density. The compositions of aggregates are presented in Table 1, which indicate that SiO_2 and Al_2O_3 were the main components in the CLWA and SLWA (devoid of calcium). In order to know the crushing resistance strength of the two types of LWAs, a number of the CLWA pellets and SLWA cubes (cubic particles cut from bulk shale) with a size/diameter of around 5 mm were tested. The crushing resistance of the CLWA pellet was calculated based on a method reported in previous studies [51, 52]. The average strength results are shown in Table 2, which also lists other physical properties of the LWAs. The total and open porosities of the two aggregates were measured by submerging them in water under vacuum for 24 h [53]. It is found that the SLWA had a far higher strength than the CLWA despite they had similar porosities. The water absorption and apparent density values of the two LWAs after soaking in water for 24 h were similar (under ambient condition). The pre-wetted density of the SLWA was slightly higher than that of CLWA, whereas the dry bulk density of the former was a little lower.

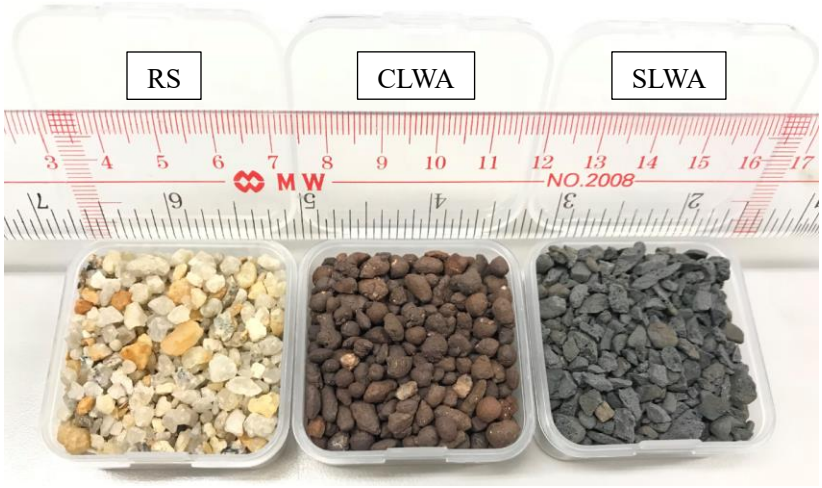

Fig. 2. Appearances of RS, CLWA and SLWA used in this study.

Table 2. Physical properties of LWAs.

Physical properties	CLWA	SLWA
Crushed resistance (N/mm^2)	0.76	4.58
Open porosity (%)	20.5	18.7
Total porosity (%)	68.0	63.9
Water absorption (24 h soaking in water, %)	13.4	14.2
Apparent density (24 h soaking in water, kg/m^3)	956	1065
Loose bulk density (Dry, kg/m^3)	539	525

2.2 Mix proportions and research framework

The HPLAC mixtures were comprised of two parts, one was a UHPC paste and the other was LWAs. The mix proportions of HPLAC mixtures are listed in Table 3. The pozzolans with different particle sizes were combined to prepare a high performance paste. For the reference mixture (100R), the natural RS was adopted as an aggregate and then compared with the LWAs. The aggregate-to-binder ratio was set as 1:1 by mass. A *w*/*b* ratio of 0.17 was used for the reference mixture. Since the LWAs would absorb water during mixing, they were pre-soaked in water for 24 h [54], and then the LWAs were used to replace 50% and 100% RS by volume. Since part of water would be released from pre-soaked LWAs due to the centrifugal force during the high-speed mixing [55], the *w*/*b* of HPLACs was reduced slightly (Table 3) to maintain a similar

flow value with the reference mixture (180±5 mm determined by flow table [56]). To further reduce the weight of the mixture, more pre-wetted LWAs (150% and 200% volume of RS based on the reference mixture) were introduced into the mixture. For all the mixtures, the dosage of a polycarboxylate ether (PCE) superplasticizer (BASF, SKY 8588) was 3% of the binder by mass. The water content in the superplasticizer was 80%. Short straight steel fibers coated by copper (diameter of 0.22 mm and a length of 13 mm) were employed to reinforce the samples. As the addition of the steel fibers with very high density would increase the weight of concrete largely, the dosage of the fibers was controlled at 1.5% by the paste volume. The number in the codified mix refers to the percentage of aggregates. The 'C' and 'S' denote the CLWA and SLWA, respectively. For example, the 100C means that the mixture was prepared with 100% CLWA as aggregates.

Table 3. Mix proportions of HPLACs prepared with SLWA and CLWA (kg/m^3).

Mix	Cementitious materials				Fiber	PCE	Aggregates			Water	*w*/*b*
	OPC	SF	MK	GGBS			RS	CLWA	SLWA		
100R	827	124	41	83	61	32	1075	/	/	157	0.17
50C	827	124	41	83	61	32	537	203	/	146	0.16
100C	827	124	41	83	61	32	/	406	/	135	0.15
150C	687	103	34	69	51	27	/	506	/	113	0.15
200C	584	88	29	58	43	23	/	574	/	96	0.15
50S	827	124	41	83	61	32	537	/	226	146	0.16
100S	827	124	41	83	61	32	/	/	452	135	0.15
150S	687	103	34	69	51	27	/	/	564	113	0.15
200S	584	88	29	58	43	23	/	/	639	96	0.15

For the preparation of HPLACs, the cementitious materials were dry-mixed for 3 minutes in a laboratory mechanical mixer. Then, water and superplasticizer were added followed by further mixing for 6 minutes. After the mixture was turned into a paste, the RS/pre-soaked LWAs were poured into the mixer and the whole mixture was continued mixing for another 2 minutes. Then, the steel fibers were added followed by 1 minute of additional mixing to obtain a homogenous fresh mixture. After casting into steel molds, a laboratory vibrating table was used to compact the mixtures. Plastic sheets were used to cover the surface of mixtures to avoid moisture loss. 24 h later, the specimens were demoulded and cured in a water tank (25±2 ºC) for different periods before testing.

2.3 Methods

2.3.1 Chapelle test

The Chapelle test is used for assessing the reactivity of pozzolanic materials in cement-based systems [57, 58]. In this study, the pozzolanic activity of the LWAs was evaluated by this method. One gram of the powdered aggregate (RS, CLWA, and SLWA) was allowed to react with one gram of $Ca(OH)_2$ in 200 mL distilled water. The prepared solution was placed in sealed glass bottles and heated to 80 °C and kept for 16 hours. After cooling down to room temperature, 20 grams of sucrose were added to dissolve the remaining unreacted $Ca(OH)_2$, with the aid of magnetic stirring for 20 mins to make sure the complete complexion of the Ca ions. Afterward, the suspensions were filtered through 2.5 μm filter papers using vacuum filtration. 0.1 N HCl and methyl orange indicator were employed to titrate the filtered solution. Thus, the remaining and reacted $Ca(OH)_2$ amounts could be calculated based on the consumed HCl dosage. The reactivity of the aggregates was then obtained as the consumed $Ca(OH)_2$ amount by the aggregates divided by the original $Ca(OH)_2$ amount. After drying the solid residues (obtained from filtration) at 105 °C, a thermogravimetric (TG, Rigaku Thermo Plus EVO2) analysis was conducted to obtain the bound water of the residues [59].

2.3.2 Physical properties

The compressive strength of the samples was measured at 7, 28, and 90 days of curing following ASTM C109 [60]. Samples with the size of 40×40×40 mm^3 were prepared for measurements. A compression machine with a maximum force of 3000 KN was used for testing. The loading rate for the test was set as 0.6 MPa/s. Three specimens were measured for obtaining an average value. The wet density of the samples was also tested at different curing times. The volume of the samples was measured by a water displacement method based on BS EN 12390-7:2019 [61]. The mass of the samples was weighted in the saturated surface dry (SSD) condition. Besides, the water absorption of the 90 days samples was measured according to ASTM C642 [62]. Before recording the dry mass, the samples were dried in a ventilated oven at 105 °C until constant mass was achieved.

228 2.3.3 Thermal conductivity

229 The thermal insulation property of HPLACs was assessed by a thermal conductivity test. Samples
230 with a dimension of 40×40×40 mm^3 were used for testing after curing at 28 and 90 days. A thermal
231 conductivity meter equipped with a Hot Disk Kapton sensor was employed for the measurements.
232 The measurement range of the device was from 40 down to 0.03 W/m/K. The temperature during
233 the measurement was 21 ºC. At least five samples from each mixture were tested to obtain an
234 average value.

235

236 2.3.4 Isothermal calorimetry

237 The isothermal calorimetry was tested to monitor the hydration kinetic of HPLACs prepared with
238 pre-soaked LWAs. The hydration heat of samples containing different amounts of the SLWA was
239 recorded and the cases of 100R and 100C were also tested to make comparisons with the SLWA-
240 incorporated samples. The proportions of the samples complied with Table 3. The fresh mixtures
241 located in insulated containers were transferred to an isothermal calorimeter (Calmetrix I-CAL)
242 for measurements. The heat of hydration was monitored up to 168 h at a constant temperature of
243 20 ºC.

244

245 2.3.5 Durability related properties

246 The ion permeability of 100R and 100S was determined to evaluate the concrete's resistance to
247 chloride-ion penetration according to ASTM C1202 [63]. This rapid electricity flux method has
248 been widely used for characterizing the permeability of high strength lightweight concrete [9, 19],
249 although it is not without limitations [64]. The 28 days cured samples were used for testing. Slice
250 samples of 50 mm thickness were cut from cylinder concrete samples. Before testing, the samples
251 were vacuumed for 3 h, followed by saturated in water for 18 h. A voltage of 60 V was exerted on
252 a cell with one side filled with 3% NaCl solution and the other side 0.3 M NaOH solution. The
253 total charge passed after 6 h was recorded as an indication of chloride ion penetrability.

254

255 The autogenous shrinkage of 100R and 100S was measured using the corrugated tube method
256 according to ASTM C1698 [65]. The fresh mixtures were filled into polyethylene tubes (420 mm
257 in length and 29 mm in outer diameter) held vertically while the vibrating table was switched on.
258 The measurement of autogenous deformation was started after setting and continuously monitored
259 for 14 days under the sealed condition at 23 ºC. The data were recorded every minute during the

testing period.

2.3.6 Microstructure tests

X-ray diffraction (XRD, Rigaku SmartLab-Advance) equipped with a 9 kW rotating anode X-ray source (λ~1.54Å) was employed to identify the mineralogy of the aggregates (RS, CLWA, and SLWA). A high quality semiconductor detector (HyPix-3000) was used to scan the powdered samples. The scan ranged from 10° to 70° in this measurement with a scan speed of 5 °/min and a 0.01° step size. To quantify the crystal phases in the aggregates, 20 wt% of corundum was added to the samples as an internal standard. Rietveld refinement was conducted to analyze the data by using Topas 4.2 software.

A mercury intrusion porosimeter (MIP, Micromeritics AutoPore IV 9500) was adopted to analyze the pore structure of LWAs. Pores with sizes from 360 μm down to 5 nm could be measured via the intrusion of mercury into the connected pores under an intrusion pressure of up to 227 MPa. The pore shapes were assumed to be cylindrical and the contact angle of the mercury on the solid surface was taken as 140° [66]. Despite the debate using MIP for measuring porosity due to the irregularity of pore geometries and ink-bottle effects [67], the information obtained is still useful for qualitative analysis and comparison [53]. The surface of the raw LWA particles and their interior structure were observed using a scanning electron microscope (SEM, Tescan VEGA3). The backscattered electron (BSE) imaging mode was performed on the carbon-coated polished cross section of LWAs to explore the internal pore connectivity in the LWAs. The pores in the LWAs were filled with epoxy and then the samples were polished before BSE observation. For the concrete samples, the cube samples after 90 days curing were cut into slices and then embedded in epoxy and polished by the different fineness of papers (180 grits, 9 μm, 3 μm, 0.05 μm). After obtaining a smooth surface, the samples were cleaned in ethanol in an ultrasonic bath for 5 mins to remove the residual suspensions on the surface. Before the BSE testing, the samples were dried in a 40 °C vacuum oven for 3 days and coated with carbon for conduction. Energy-dispersive X-ray spectroscopy (EDX) was conducted to analyze the elemental distribution of the matrix. The above SEM/BSE observations were carried out under 20 kV voltage.

Fig. 3. Indentation areas in 100R, 100C and 100S.

A Bruker's Hysitron TI Premier nanoindenter was employed to measure the micromechanical properties of the interfacial zone between the aggregate and the paste. A square indentation grid of 400 points (20 × 20) was programmed for the indentation (see Fig. 3) and the interval distance between the grids was 5 μm. A trapezoid loading program was used for the measurement. The indentation force was loaded up to a maximum value of 2000 μN at a rate of 400 μN/s using a diamond tip with Berkovich triangular pyramidal. Then, the maximum force was held for 2 s, followed by unloading within 5 s. The hardness and elastic modulus of the indented points were obtained according to the depth-load curves [68, 69]. The preparation of samples (90 days of curing) for the nanoindentation test was similar to that of the SEM-BSE testing. However, to achieve a very smooth surface, the samples were further polished by fine grits (9 μm, 3 μm, 0.05 μm) for 30 mins, respectively.

The pore structure in the paste of HPLACs was evaluated by the Brunauer-Emmett-Teller (BET) test (the MIP method would involve the information of pores in LWAs). A porosimetry instrument with a two-station degas system (Micromeritics ASAP 2020) was used for nitrogen adsorption and desorption. Small fragments (75-315 μm) crushed from the 90 days cured samples were used in this test. The steel fibers in the samples were removed by a magnet. The vacuum degassing temperature was set at 60 °C to remove the remaining water from the smallest pores, followed by an analysis procedure under liquid nitrogen conditions. Pore information in the range of 2-100 nm could be obtained from this measurement. Since the HPLACs contained LWAs, the actual pore information of the paste matrix was calculated by subtracting the pores in the LWAs in the samples.

A high resolution X-ray computed tomography (μCT, YXLON FF35) was employed to observe the distributions of LWAs and fibers in the HPLACs in a non-destructive way. 40×40×40 mm^3 cube samples were used for CT scanning and the internal voids in the LWAs (about 5 mm in

diameter) were also detected. The X-ray tube was operated at 200 kV voltage and 65 μA current for the concrete samples and 100 kV voltage and 60 μA current for the LWA particles. For both samples, 1800 projections of two-dimensional (2D) images were captured in a 360° rotation with an integration time of 1.67 s. 0.1 mm tin and 0.1 mm copper were taken as filters for concrete and LWAs samples, respectively. The three-dimensional (3D) volumetric structures were generated via real time reconstruction software (CERA). Then, the 2D and 3D CT images were visualized and analyzed by VGStudio MAX.

3 Experimental results

3.1 Physicochemical properties of LWAs

3.1.1 Mineralogy of LWAs

The XRD spectra of the different aggregates are displayed in Fig. 4. As seen, the distinct peaks of quartz were identified in all aggregates. However, the intensity of the quartz signal was strongest in the RS, and lowest in the shale-based SLWA. To some extent, this implies the highest content of quartz in the RS and the lowest content of quartz in the SLWA. The results are consistent with the Q-XRD analyses shown in Table 4, which presents that the order of quartz content was RS (sand)＞CLWA (clay)＞SLWA (shale). On the other hand, the amount of amorphous phases in the aggregates followed the sequence: SLWA＞CLWA＞RS. From the diffractograms, hercynite ($FeAl_2O_4$, PDF#34-0192) was also observed as crystal phase in the LWAs and its content was slightly higher in the CLWA than that in the SLWA (see Table 4). Zhang and Gjørv also compared the mineral compositions of various LWAs (including Liapor, Leca, and Lytag), they found different minerals in the various LWAs due to the completely different raw materials and manufacturing procedures [70]. In this study, although the two types of LWAs were produced with different raw materials (clay and shale), they still had similar chemical and mineral compositions. However, the fraction of each mineral in the two types of LWAs was different, which might induce different chemical reactivities. As indicated by previous studies [70, 71], the LWAs possessed some pozzolanic reactivity due to the high temperature manufacturing process (typically in the range of 1000-1200 ºC [72]). The ions (e.g. Al and Si) released from the LWAs would react with $Ca(OH)_2$ to form additional hydrates [71, 72]. Hence, the higher content of amorphous phases revealed that the LWAs would likely involve in the pozzolanic reaction with

the surrounding paste.

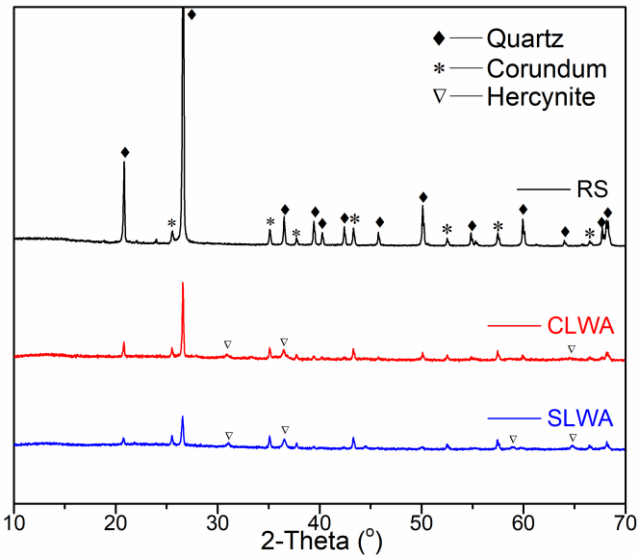

Fig. 4. XRD patterns of the RS, SLWA and CLWA (with 20 wt.% corundum).

Table 4. Phase contents in the aggregates analyzed by Q-XRD (wt%).

Aggregates	RS	CLWA	SLWA
Quartz	89.9	31.8	15.0
Hercynite	-	9.7	8.3
Amorphous	10.1	58.5	76.7

3.1.2 Pore structure of LWAs

The pore structures of the LWAs measured by MIP are presented in Fig. 5. The pore size of the SLWA was much smaller than that of the CLWA. Most of the pores in the CLWA were larger than 1 μm, while the pores in the SLWA were mainly smaller than 1 μm. The MIP results indicate that the SLWA had a much finer pore structure than the CLWA. As indicated in ref. [53], the density and water absorption process of LWAs were related to their pore structures. Pores larger than 1 μm in the LWAs would be saturated rapidly but the absorbed water was desorbed easily, while water in smaller pores was sorbed and desorbed more slowly [55]. Therefore, it is anticipated that the internal curing effect provided by the SLWA would be adequate due to the steady and gradual water desorption. In any case, however, a large number of pores in the LWAs could provide spaces to accommodate water for internal curing. Moreover, the fine and uniform pore structure in the SLWA might account for its higher crushing strength as compared to that of the CLWA (Table 2).

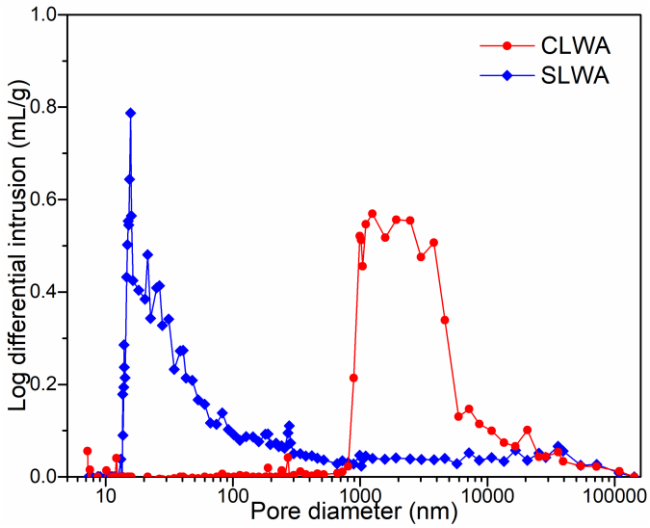

Fig. 5. Pore size distributions of SLWA and CLWA.

In order to closely examine the structure of the two lightweight aggregates, SEM-BSE was employed to observe the surface and internal pores. The appearance of the CLWA surface shown in Fig. 6a was full of cavities, but the cavities seemed to be non-connected. From the cross-section of the CLWA, an outer shell of about 500 μm thick can be identified in Fig. 6b. This relatively denser shell covered the internal pores, whose sizes were much larger than the pores in the shell. These behaviors are in line with the observation of another study [53], which showed that the outer shell of expanded clay aggregates was much less porous than the interior. Fig. 6c shows the pores of the SLWA. As the SLWA was crushed from the big bulk of expanded shale, the surface was very rugged and the pores were opened. A close examination in Fig. 6d displays that the surface pores with different sizes were separated by the shale matrix. Zhang and Gjørv [73] found that the penetration of cement paste into LWAs depended on the surface of the LWAs. The cement paste did not penetrate through the dense shell, while it could penetrate into the opening pores of surface. Hence, for the SLWA, the bond was expected to be better due to an improved mechanical interlocking between the aggregates and the cement paste.

BSE images of the polished cross-section in Fig. 7 show the interior pores in the CLWA and SLWA. For the CLWA (Fig. 7a), a clear shell in the outer part of the aggregate was observed. In contrast, the interior structure in the CLWA was observed more porous. As shown in Fig. 7b with greater details, many interior pores were well-interconnected or separated by a thin wall. This characteristic of pore structure was prone to water absorption and storage. However, the large voids

inside the CLWA would make the aggregate weak and friable [53]. Figs. 7c and 7d present the interior structure of the SLWA. The cross-section images demonstrate the open-cell pores on the surface of the particle. In comparison with the CLWA, the interior pores in the SLWA were more isolated, and the walls between the pores were thicker. The refinement of the pore structure might be responsible for the higher strength of the SLWA compared to the CLWA (see Table 2). Additionally, the open pores of the SLWA could increase the bonding area with the paste and reinforce the interfacial pozzolanic reaction, in contrast, the densely sintered shells on the surface of the CLWA would lower chemical reactivity. The surface structure of SLWA was similar to that of Lytag (sintered fly ash) without a dense shell, which facilitated to form a more dense and homogeneous ITZ [74]. For the LWA with a dense shell, some crystalline hydration products, such as $Ca(OH)_2$ and ettringite, would accumulate at the dense outer layer to make the ITZ more porous [74]. As a consequence, although the two types of LWAs had similar porosities (Table 2), they had different pore structures and geometries, both of them affecting the overall strength of HPLACs by processes which took place in the ITZ.

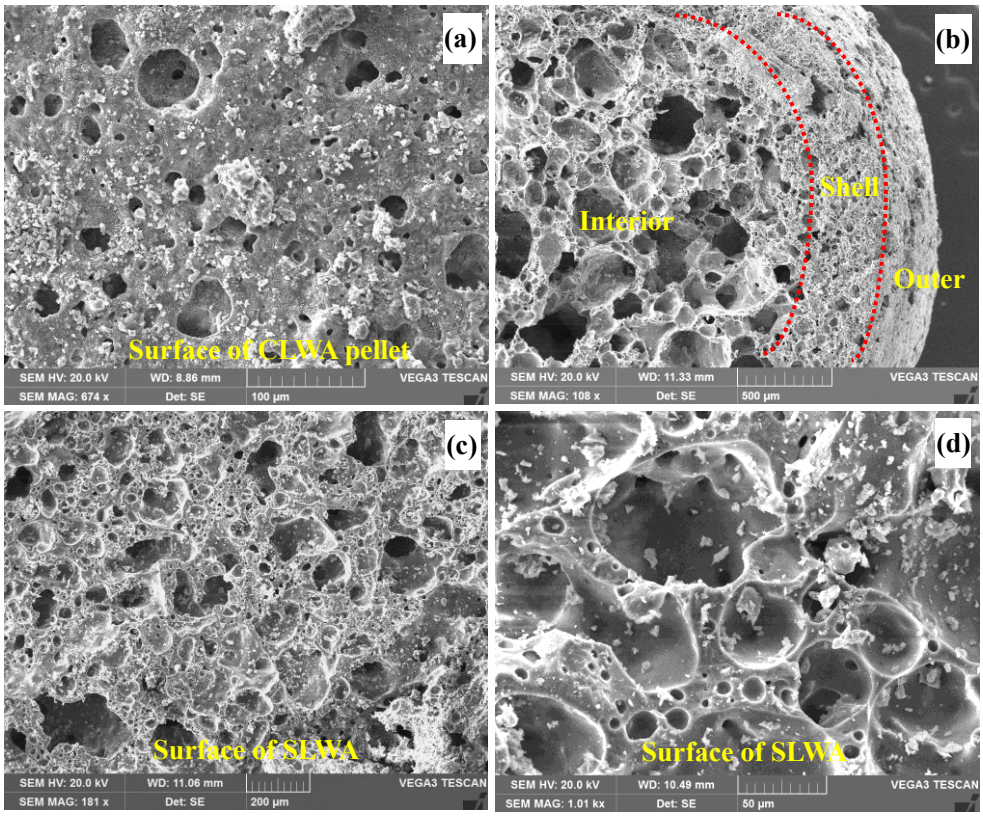

Fig. 6. SEM of pores in the CLWA and SLWA, (a) surface of CLWA; (b) internal pores of CLWA; (c) and (d) surface pores of SLWA.

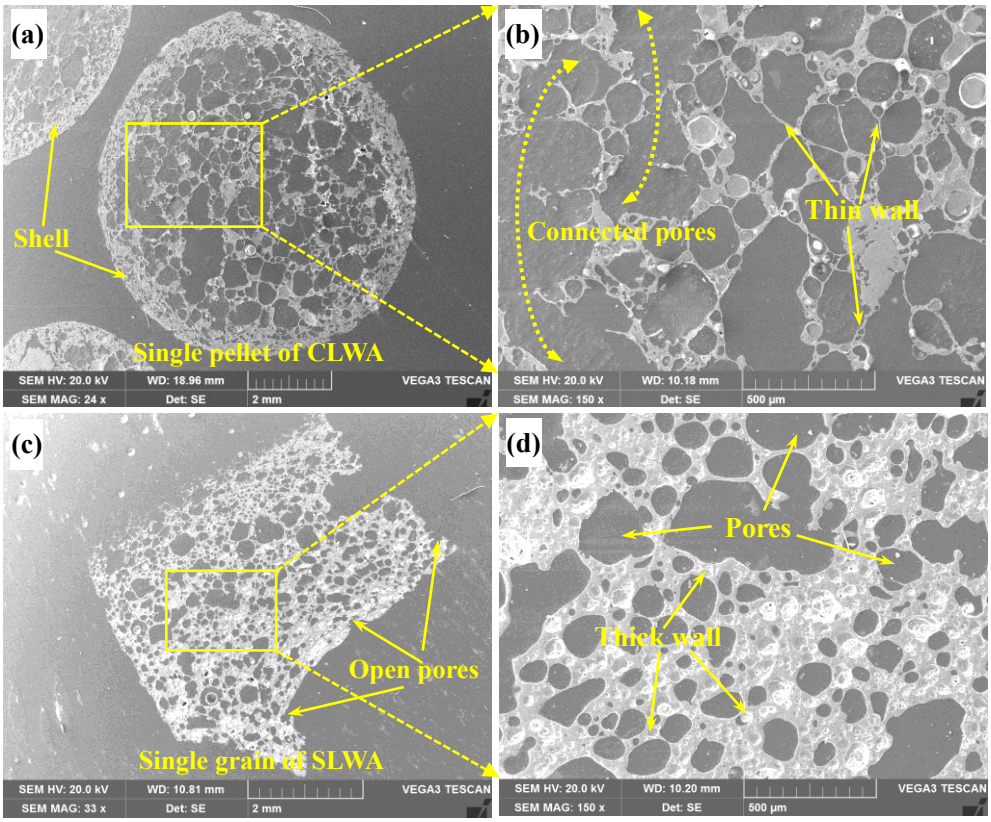

Fig. 7. BSE images of internal pores in the CLWA and the SLWA, (a) cross section of CLWA; (b) magnification of (a); (c) cross section of SLWA; (d) magnification of (c).

3.1.3 Pozzolanic reactivity of LWAs

To assess the possible pozzolanic reactivity of the CLWA and SLWA in the alkaline cementitious system, Chapelle test was performed to obtain calcium hydroxide (CH) consumption by the different aggregates (which were in powdered forms). Fig. 8a shows that the RS had the least value of CH consumption and the SLWA consumed the highest amount of CH, which means that the SLWA possessed the highest pozzolanicity among the tested aggregates. Accordingly, the SLWA had a higher material activity than the CLWA. Since the SLWA was processed by rapid cooling from high temperatures and mainly composed of SiO_2 and Al_2O_3, it could be possible that Al and Si would be released from the SLWA to react with CH [71]. It should be noted that per gram of the SLWA could react with 527 mg CH, which is similar to that of a typical pulverized fly ash (classified as a highly reactive SCM) [57]. Also, Kong et al. [72] investigated the chemical reactivity of LWAs (sintered fly ash and expanded clay/shale) and found that the finely ground LWAs had similar pozzolanic reactivity with fly ash. The powdered expanded slate and shale aggregates were also found to have pozzolanic nature, the consumption of CH was comparable to

or higher than fly ash [75]. Tasong et al. [76] indicated that the natural aggregates were chemically active and the ions released and absorbed by the aggregates possibly took part in the hydration of the surface layer. Therefore, the result obtained implies that the studied SLWA would exert a high/moderate pozzolanic reaction at the interfacial zone in the cement-based matrix. Certainly, the LWAs in the form of powder should be more reactive than in the form of coarse aggregates, thus if the SLWA was ground into powder form, it may be used as a potential SCM. From Fig. 8b, it can be seen that the residue of the reacted samples experienced a severe mass loss from 100 to 300 °C. Thus, the bound water of the residual samples of RS, CLWA, and SLWA calculated in this temperature range was 13.0%, 19.4%, and 24.8%, respectively. These results further confirmed that the order of pozzolanic reactivity among the aggregates was SLWA＞CLWA＞RS. On the other hand, this sequence indicates that the larger amounts of Al and Si were released from the SLWA and reacted with CH to form hydration products compared to the CLWA.

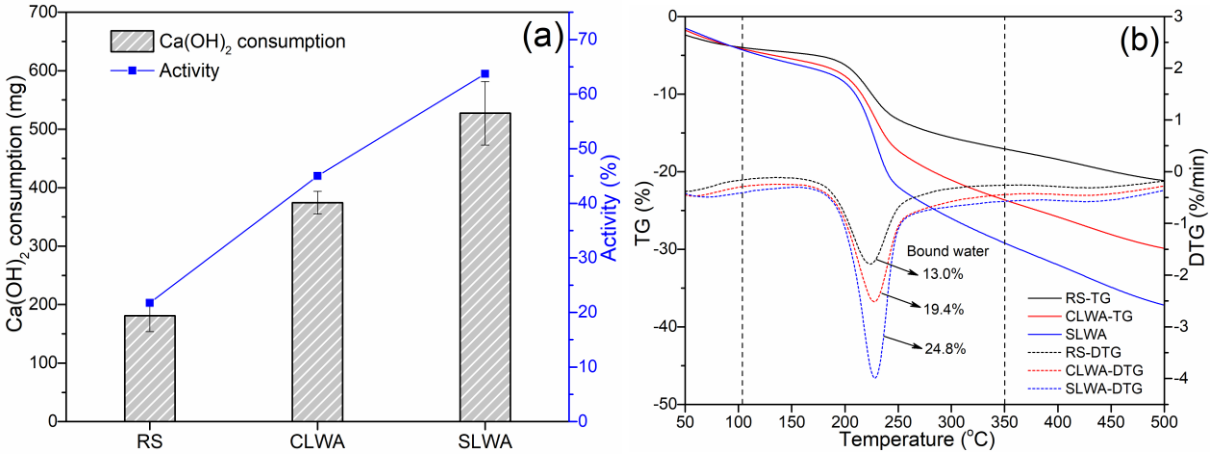

Fig. 8. Pozzolanic reactivity of aggregates determined by Chapelle tests, (a) Consumptions of $Ca(OH)_2$ by per g of aggregate; (b) TG/DTG analyses of residual solids after Chapelle tests.

3.2 Physical and functional properties

3.2.1 Density and water absorption

The density and water absorption values of HPLACs are shown in Fig. 9. With the incorporation of the two types of LWAs, the density of samples was reduced significantly, in particular when the RS was fully replaced by the LWAs (Fig. 9a). With further increase in the content of LWAs, the reductions in the density were not remarkable, regardless of the samples prepared with the CLWA

and SLWA. Since the density of RS was much higher than those of LWAs (see Table 1), the density of the samples dropped significantly to around 1850 kg/m^3 by replacing 100% RS. A recent study [77] also reported a similar density with the use of SLWA in the concrete, regardless of quasi-spherical shale and crushed shale. In general, the density of lightweight concrete is associated with the density of LWAs. If the LWAs with low density were used, the lower overall density of concrete would be attained. Therefore, some studies [78-80] incorporated very lightweight materials (e.g. aerogel, straw and expanded polystyrene) into the UHPC system to reduce the density and ensure the high strength. However, with the reduction in the density, the strength of lightweight concrete would be reduced inevitably. In this study, the influence of these two types of LWAs on the reduction of density seemed to be similar. This is because the pre-wetted densities of the CLWA and SLWA were similar (0.96 vs 1.1 g/cm^3).

Water absorption is an essential factor which is primarily related to the durability of the concrete. Fig. 9b presents the water absorption of HPLACs prepared with the two types of LWAs. In both cases, the water absorption of the samples was increased with the increasing content of the LWAs. Especially for the CLWA containing samples, the water absorption was increased significantly with the decrease in density. Furthermore, the inclusion of the porous expanded clay aggregates with interconnected pores might have a negative effect on water retention. This result is in agreement with the findings of other works [28, 81], which indicated that the replacement of natural aggregates by LWAs and the increased amount of LWAs in the mixture increased the water absorption of the lightweight concrete. However, in this study, the water absorption values of HPLACs were still much lower than those of conventional lightweight concrete [81, 82] and normal weight cement mortar and concrete [83, 84] (mostly＞7%). As the water absorption was less than 5%, the HPLACs prepared in this study were expected to have a good quality [28]. By contrast, the increase of water absorption of the expanded shale-based samples was not significantly changed with the increasing aggregate content. The results mean that the HPLACs prepared with the SLWA had a more compact structure than those prepared with the CLWA at a similar level of density.

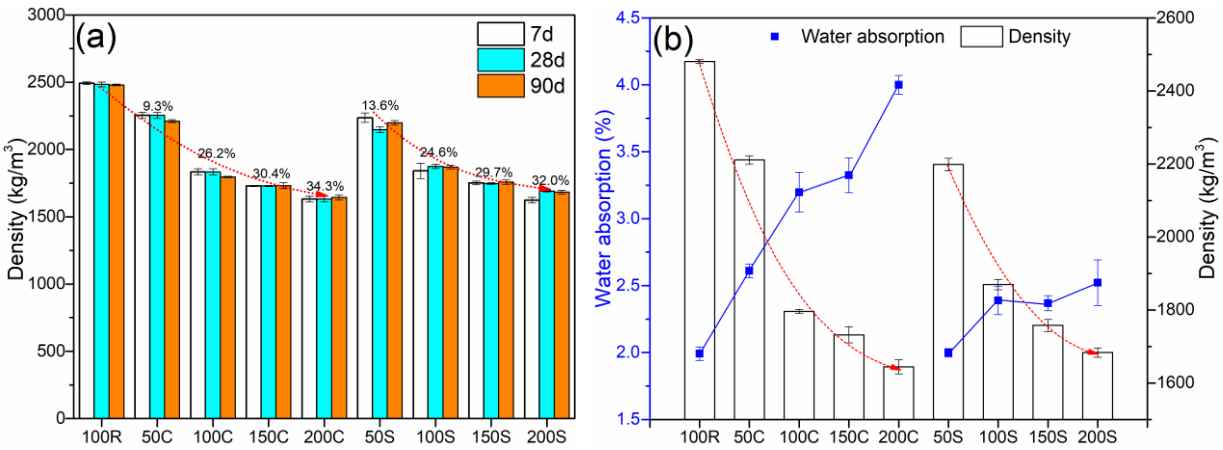

Fig. 9. SSD density (a) and water absorption (b) of HPLACs.

3.2.2 Structural efficiency

The compressive strength and corresponding structural efficiency of HPLACs are presented in Fig. 10. When the LWAs were used to replace RS, the compressive strength was reduced considerably due to their intrinsic weak strength. In particular, a large reduction in the strength was observed in the case of the CLWA-incorporated samples. The strength of the 100C dropped by 70% as compared with the reference sample at 90 days. Further increasing the content of the CLWA only slightly reduced the strength. This might be due to the fact that the large proportion of the CLWA had formed a network packing in the matrix to stabilize the strength reduction. For the HPLACs prepared with SLWA, the reduction of strength appeared to be less pronounced in comparison with the CLWA system, especially when the RS was fully replaced by the SLWA. The strength was substantially higher than those of the CLWA samples. A high strength exceeding 70 MPa could still be achieved for the 100S. Based on the results of ref. [77], the use of the crushed shale LWAs in concrete could attain higher strength than the use of the quasi-spherical shale LWAs because the angular shape and rough surface of the LWAs could provide a better bonding with the cement paste. Hence, the SLWA with open-pore surface in this study might contribute to the high strength as compared to the CLWA. With the increase of the SLWA content, the strength decreased as expected.

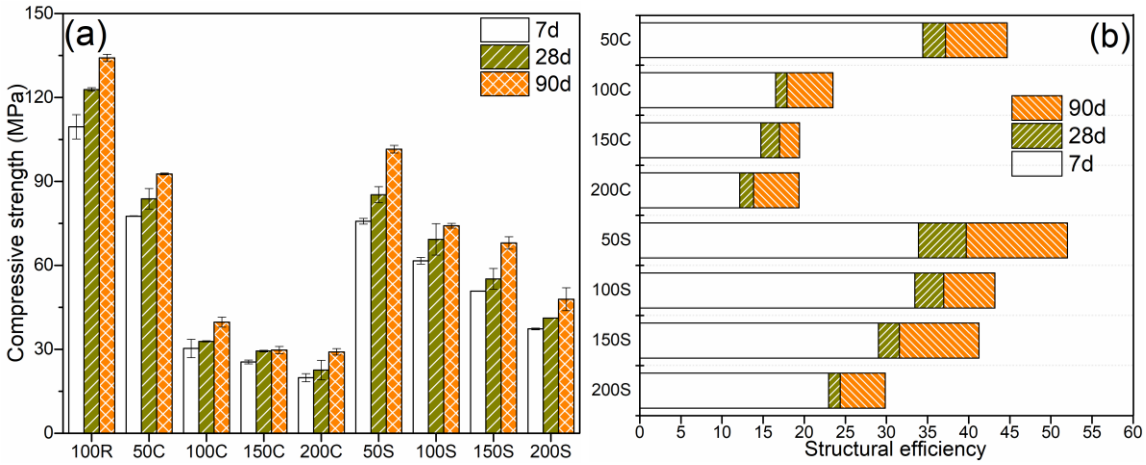

Fig. 10. Compressive strength (a) and structural efficiency (b) of HPLACs.

Structural efficiency (strength/density, kN·m/kg) is a parameter to represent the material efficiency for lightweight concrete. The higher value means a higher efficiency to reduce the dead load of the concrete structures and vice versa. Fig. 10b shows the structural efficiency of HPLACs prepared with two kinds of LWAs. The results indicate that the structural efficiencies of HPLACs prepared with SLWA were obviously higher than those of the CLWA incorporated samples. Therefore, the introduction of the SLWA in the HPLACs was more effective in reducing the structures' weight at the same grade of density compared to the use of the CLWA. Several physicochemical properties of the SLWA may be responsible for this behavior: (i) the finer pore structure of the SLWA (see Section 3.1.2) resulted in a higher aggregate strength (see Table 2); (ii) the open-pores surface of the SLWA (see Section 3.1.2) were conducive to improving the bonding between the aggregates and the paste (to be discussed in Section 3.3.2); (iii) the coupled effects of internal curing and high pozzolanic activity of the SLWA facilitated to form good bonds with the paste to partly counteract the weak strength of the aggregates (to be discussed in Section 3.3.3). However, it is found that the structural efficiency of the SLWA-containing HPLACs decreased significantly with the increased amount of the SLWA. This is because the strength was reduced largely while the density did not decrease too much. Another reason might be due to the incorporation of relatively larger size of the SLWA in the mixture. As reported by previous studies [34, 85], the use of LWAs with small size resulted in a higher compressive strength of lightweight concrete. This finding was confirmed by our recent work [8], which incorporated micro-sized lightweight materials into UHPC system to achieve very high structural efficiency (＞65 kN·m/kg).

3.2.3 Thermal conductivity

The thermal conductivity test results are shown in Fig.11a. The reference sample (100R) had a high thermal conductivity (2.32 W/mK at 90 days) due to the use of quartz sand with very high thermal conductivity (18.37 W/mK [86]). The replacement of the RS by the LWAs reduced the thermal conductivity remarkably. For the 100C and the 100S, the thermal conductivity values were reduced by 68% and 62% in comparison with the reference sample, respectively. The porous structure of the LWAs hindered the conduction of heat through the matrix. Also, as the UHPC matrix was water-deficient, the absorbed water in the LWAs would be consumed by the hydration of the surrounding UHPC matrix (internal curing effect) [87]. Therefore, the empty pores in the LWAs with an extremely low thermal conductivity (0.026 W/mK for air) was beneficial to lowering the thermal conductivity. This explanation is also supported by the lower thermal conductivity at the longer hydration time (90 days of curing age). For the HPLACs prepared with the LWAs, the thermal conductivities seemed to be similar at the same aggregate content, which is due to the similar porosity of the CLWA and the SLWA (see Table 2). When the content of the LWAs was increased up to 200%, the thermal conductivity only went down a little. This trend is consistent with the development of density. The thermal conductivity also shows a linear relationship with the density value (Fig. 11b). In other words, the thermal conductivity of concrete decreased with the decreasing of mixture density. Hence, the thermal conductivity of the HPLACs was much lower than that of normal weight mortar/concrete (about 2.0 W/mK [88, 89]), implying a better heat insulation of mixture. If the HPLACs were used in the construction sector, energy consumption in the structures would be reduced indirectly. However, when the content of the LWAs exceeded 100%, the thermal conductivity tended to be stable. Thus, to ensure a high strength of concrete, a proper amount of the LWAs should be considered in the design of the HPLACs.

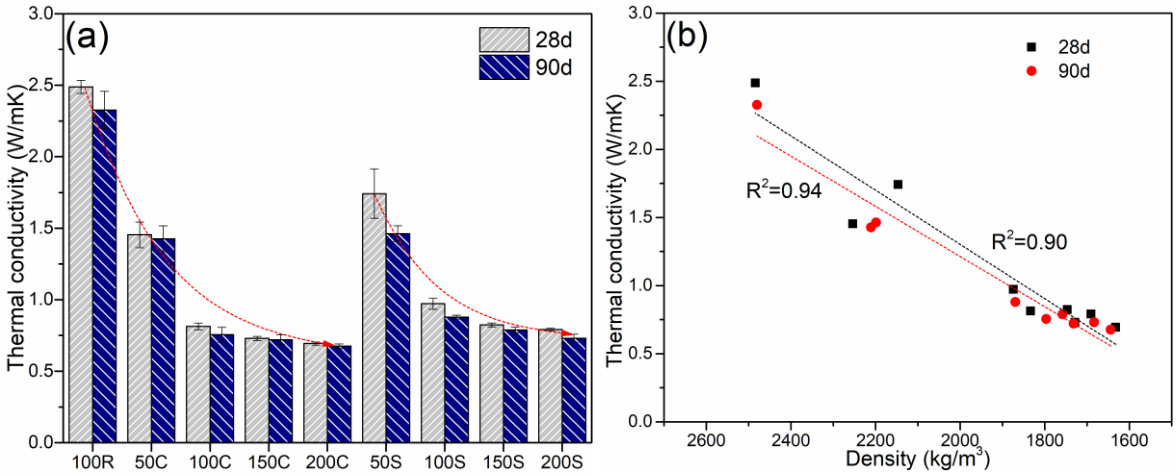

Fig. 11. Thermal conductivity of HPLACs (a) and its relationship with density (b).

528

529

530 **3.3 Hydration kinetic and microstructure**

531 3.3.1 Heat of hydration

532 Fig. 12 shows the heat flow of the HPLACs incorporated with the SLWA and CLWA as a result
533 of hydration. As demonstrated in Fig. 12a, with the use of SLWA in the HPLACs, the exothermic
534 rate of binder hydration was increased. The peak of silicate reaction was intensified with the
535 increasing amount of the SLWA, which implies the accelerating hydration due to more SLWA
536 inclusion. This result is also in agreement with a previous work [87], which showed that the heat
537 flow of mixture was closely related to the released water from the LWAs. It should be noted that
538 the LWAs were pre-soaked in water for 24 h prior to use. Therefore, the additional water available
539 in the SLWA is thought to promote the hydration of the cementitious binder. Especially for the
540 UHPC system, there were a lot of anhydrous cement clinker phases present in the matrix due to
541 the use of an extremely low *w*/*b* ratio for mixing [90]. When the internal relative humidity of
542 mixture started to decrease, the water desorption from the LWAs was triggered to maintain the
543 humidity at a high level [87]. The increased humidity in the UHPC matrix accelerated the
544 hydration of cementitious materials and delayed the occurrence of self-desiccation at the early
545 age. Another interesting phenomenon is the occurrence of an intense shoulder peak by the use of
546 the SLWA in the heat flow curve, which is usually associated with the formation of the AFm
547 phase ($C_3A{\cdot}CaSO_4{\cdot}12H_2O$) in the hydration of OPC [91, 92]. This monosulfoaluminate phase
548 was formed from the reaction of ettringite (AFt) with the remained C_3A (tricalcium aluminate)

and water [93], according to the following formula [94]. Therefore, the water released from the LWAs was able to facilitate the conversion from AFt to AFm based on Le Chatelier's principle. Our previous study [95] also validated a stronger third peak with the increasing water content in the cement paste. Another possibility for the modified peak is that ions leaching (e.g. Al) from the SLWA might enhance the intensity of the aluminate peak, similar to the effect of Al-rich metakaolin [96, 97]. As indicated, a high concentration of Al was dissolved from the SLWA in saturated limewater [71]. Hence, it is plausible that the SLWA with a higher reactivity might provide more Al for the aluminate reaction. The Al dissolution from the SLWA will be discussed in the next section.

$$C_3A{\cdot}3CaSO_4{\cdot}32H_2O\ (AFt) + 2C_3A + 4H_2O \rightarrow 3(C_3A{\cdot}CaSO_4{\cdot}12H_2O)$$

Fig. 12b shows the comparison of heat evolution between the CLWA samples and the SLWA samples. The replacement of the RS by 100% CLWA also expedited the hydration process. However, the heat flow curve of the 100C did not exhibit the aluminate peak which inferred that the presence of the CLWA suppressed the aluminate conversion. One reason may be caused by the less water was available for the conversion reaction as the water in the CLWA was released earlier due to the larger pores in the CLWA. The other possible explanation is that a less amount of Al dissolution from the CLWA was involved in the aluminate conversion. This speculation was supported by a previous study [98], which reported that the Al in the pore solution of the mixture with SLWA was higher than that with CLWA. However, further studies are needed to elucidate this phenomenon. Fig. 12c presents the cumulative heat output of the samples up to 7 days. Obviously, due to the higher exothermic heat flow, the total heat liberation was also increased with the increased amount of LWAs. It can be found that the 100S released a higher amount of heat than the 100C, which means a more profound internal curing effect of the pre-wetted SLWA than that of the CLWA. The increased contact areas of the SLWA and the paste due to the rough and open-pore surface of the SLWA might intensify the internal curing effect.

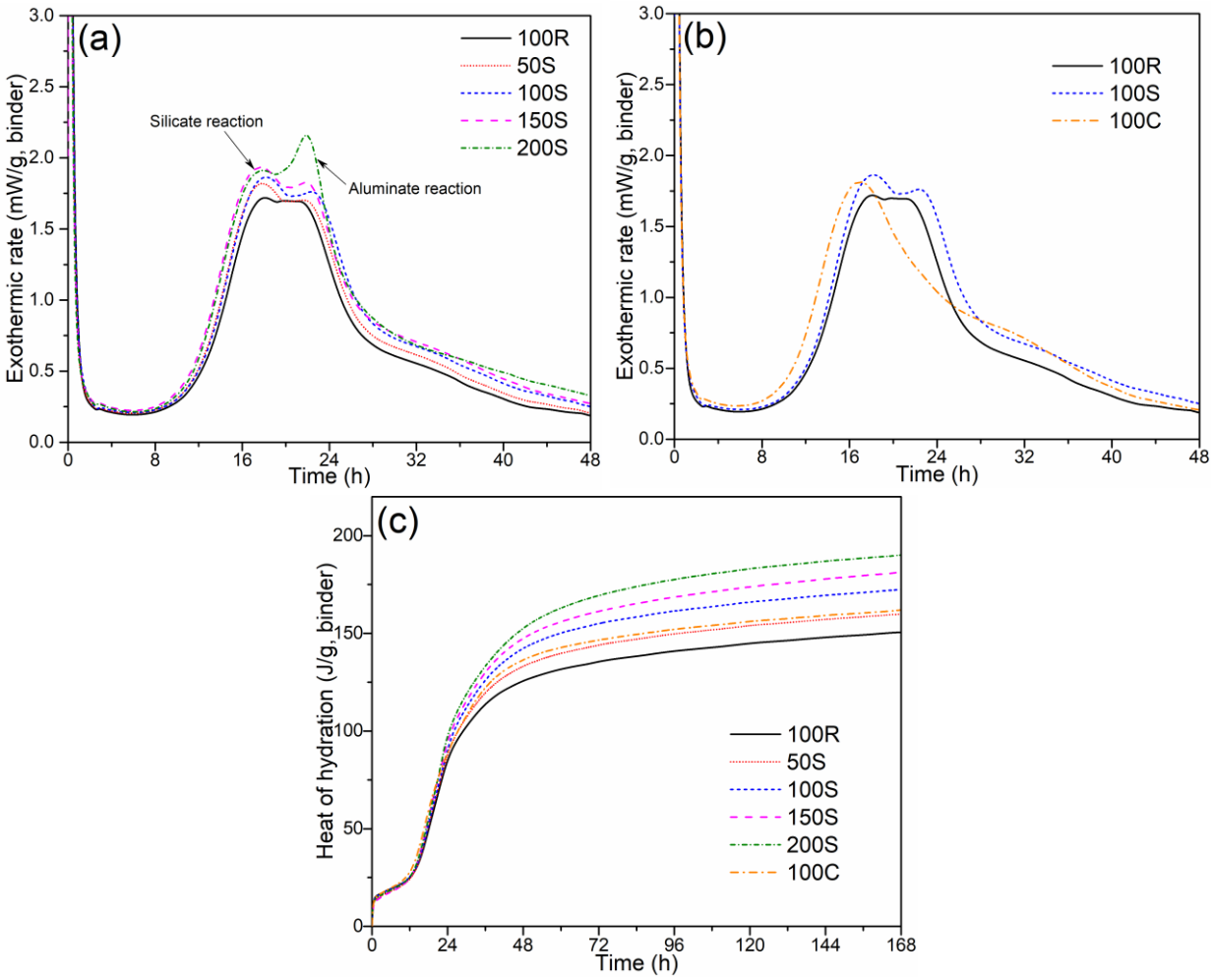

Fig. 12. Heat evolutions of HPLACs.

3.3.2 Morphology and element distribution of ITZ

The morphologies of the interfacial transition zone (ITZ) around the different aggregates are presented in Fig. 13. Distinct boundaries were found at the interface between the RS and the bulk paste (Figs. 13a and b). There were a lot of unreacted cement grains existed indicating a low hydration degree of the UHPC matrix. Figs. 13c and d show the interface of HPLACs incorporated with CLWA. The porous CLWA was surrounded by dense paste and many unhydrated cement particles were also observed in the paste. However, a close view of the ITZ reveals that fewer unhydrated cement particles were located in the immediate vicinity of the CLWA. As the CLWA was pre-soaked before use, the desorbed water could promote the hydration of the cement around the aggregates. In the HPLACs prepared with SLWA (Figs. 13e and f), the internal curing effect induced by the pre-soaked SLWA was more pronounced because the width of the ITZ (with less

unhydrated cement particles) was larger. The cement grains were turned into finer particles within the internal curing zone. This observation is consistent with the results of the hydration kinetic.

Infiltration of the paste into the cavities or open pores of the SLWA was observed (with uneven boundaries in Figs. 13e and f), which contributed to the bonding between the two phases. Similar observations were also found in other works [73, 74], for a LWA with dense outer layer, its ITZ was similar to the case of normal weight aggregate, whereas more dense ITZ was formed at the interphase of porous surface LWA. Therefore, due to the different microstructural characteristics of the two kinds of LWAs, an improved mechanical interlocking between the SLWA and the cement paste was observed. As reported by Wasserman and Bentur [99], this impregnation behavior could lead to 20% increase in strength at 90 days. In conventional LWA concrete, portlandite and ettringite were usually found to precipitate in the ITZ of LWAs [74, 100] since pre-wetting process resulted in a layer of water amassing on the surface of LWAs, which were expected to induce cracks. In this study, dense structure get rid of crystalline products deposition was observed in the ITZ of LWAs. This is because the hydropenic UHPC paste could consume most of water released from the LWAs. Zhang and Gjørv [101] also pointed out that, by reducing the *w*/*b* ratio and addition of silica fume, the ITZ of the LWAs was improved. Table 5 presents the elemental compositions of areas in the ITZ and paste matrix (Fig. 13e). The black point in the cement paste showed a high Ca/Si ratio, while the blue and red points in the internal curing zone of SLWA had much lower Ca/Si ratios. Another interesting behavior was the high concentration of Al in the ITZ of the SLWA sample, which implies the chemical interaction between the SLWA and the paste in the form of pozzolanic reaction.

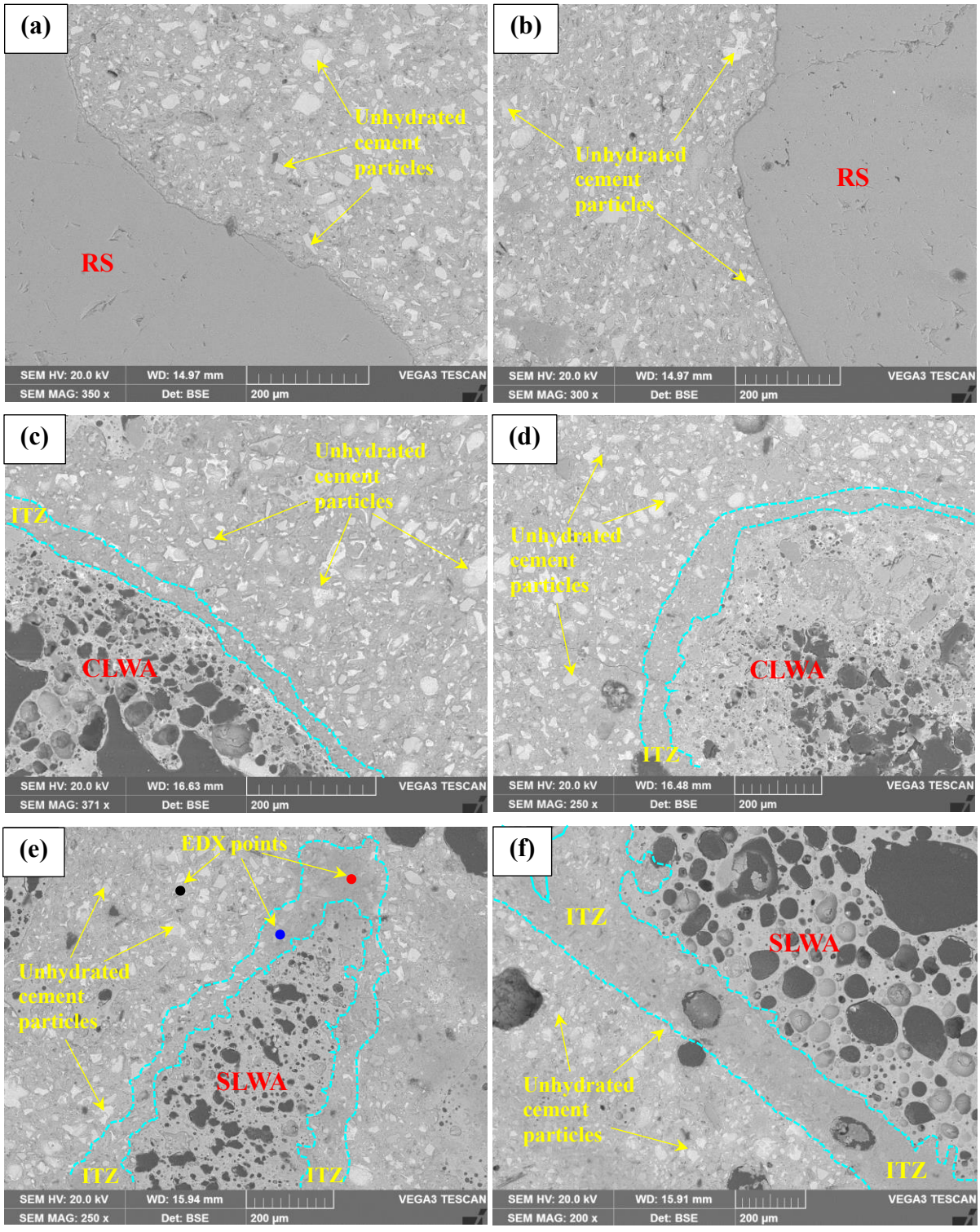

Fig. 13. SEM-BSE images of HPLACs, (a) and (b) 100R; (c) and (d) 100C; (e) and (f) 100S.

609
610

611

Table 5 Elemental compositions of EDX points.

Element	Black point	Blue point	Red point
O	71.9	70.7	70.6
Al	4.6	11.6	20.6
Si	5.6	5.5	3.5
Ca	13.1	9.6	5.1
Ca/Si	2.34	1.76	1.46
Ca/(Si+Al)	1.28	0.56	0.21

To further understand the elemental distributions at the interface of HPLACs containing CLWA and SLWA, EDX mapping was carried out and the results are shown in Fig. 14. As seen in the frame mapping of 100C (Fig. 14a), the CLWA was rich in Si and Al, but deficient in Ca, which is consistent with its chemical compositions (Table 1). At the interface, the Si and Al concentrations were observed similar to those in the bulk paste but were lower than in the CLWA. The amount of Ca in the ITZ was found lesser than that in the paste since lots of Ca-rich cement particles were located at some distance from the aggregates. The elemental distribution of ITZ by line scan is also shown in Fig. 14a. It can be noticed that the intensities of Si, Al, and Ca in ITZ were observed close to those in the hydration products. These results imply that the internal curing caused by the pre-wetted CLWA had little influence on the composition of the surrounding hydrates. Also, from the linear mapping curves, an ITZ with approximately 60 μm width can be identified (but it should be noted that the width of the ITZ would vary even with one LWA particle due to the distribution of pore structures in the LWA). Fig. 14b presents the elemental distribution of ITZ in 100S. In the frame mapping images, an interesting phenomenon can be observed: a higher concentration of Al but lower concentrations of Si and Ca in the ITZ stripe in comparison with the bulk paste. The line scanning curves clearly show the changes of concentration of these three elements from the paste to the aggregate. A width of 150 μm ITZ could be noticed based on the elemental distributions. Strong intensity of Al was observed within the ITZ with lower intensities of Si and Ca. These results are in agreement with the EDX results in Table 5. The release of Al from the SLWA was supported by other studies [71, 98], which demonstrated that the Al released from the shale-based LWA could take part in the formation of calcium-aluminosilicate-hydrate (C-A-S-H). The study of Nie et al. [71] also indicated that, as compared to the Si, the Al released from the LWA could migrate more easily and farther away from the LWA. Therefore, it can be inferred that the presence of pre-soaked SLWA changed the composition of its surrounding cement hydration products. As

638 mentioned in Section 3.1.3, the SLWA had a higher pozzolanic reactivity compared to the CLWA,
639 it is therefore suggested that the SLWA could react more intensely with the alkaline pore solution
640 to form C-A-S-H. Li et al. [98] found that both the expanded shale and clay could increase Al
641 content in the pore solution of concrete, but the expanded shale seemed to release more Al than
642 the expanded clay. This may be the reason of higher concentration of Al in the ITZ of the SLWA
643 mixture. The internal curing effect of the SLWA facilitated the cement hydration and pozzolanic
644 reaction in the ITZ. As a result, hydrates with a lower Ca/(Si+Al) ratio (Table 5) were formed in
645 the vicinity of the aggregates. Many studies [71, 102, 103] indicated that the incorporation of Al
646 in the C-S-H gel could lengthen the mean chain length of C-S-H structure, which might lead to a
647 denser microstructure and higher mechanical performance [104, 105]. Hence, the formation of the
648 additional C-A-S-H hydrates was expected to strengthen the ITZ (to be discussed in following
649 section). The reinforcement of the outer layer of the SLWA due to the continuity of the C-A-S-H
650 outside and inside the aggregates could also compensate for their lower initial strength. This would
651 be beneficial to ensuring the overall strength of concrete.

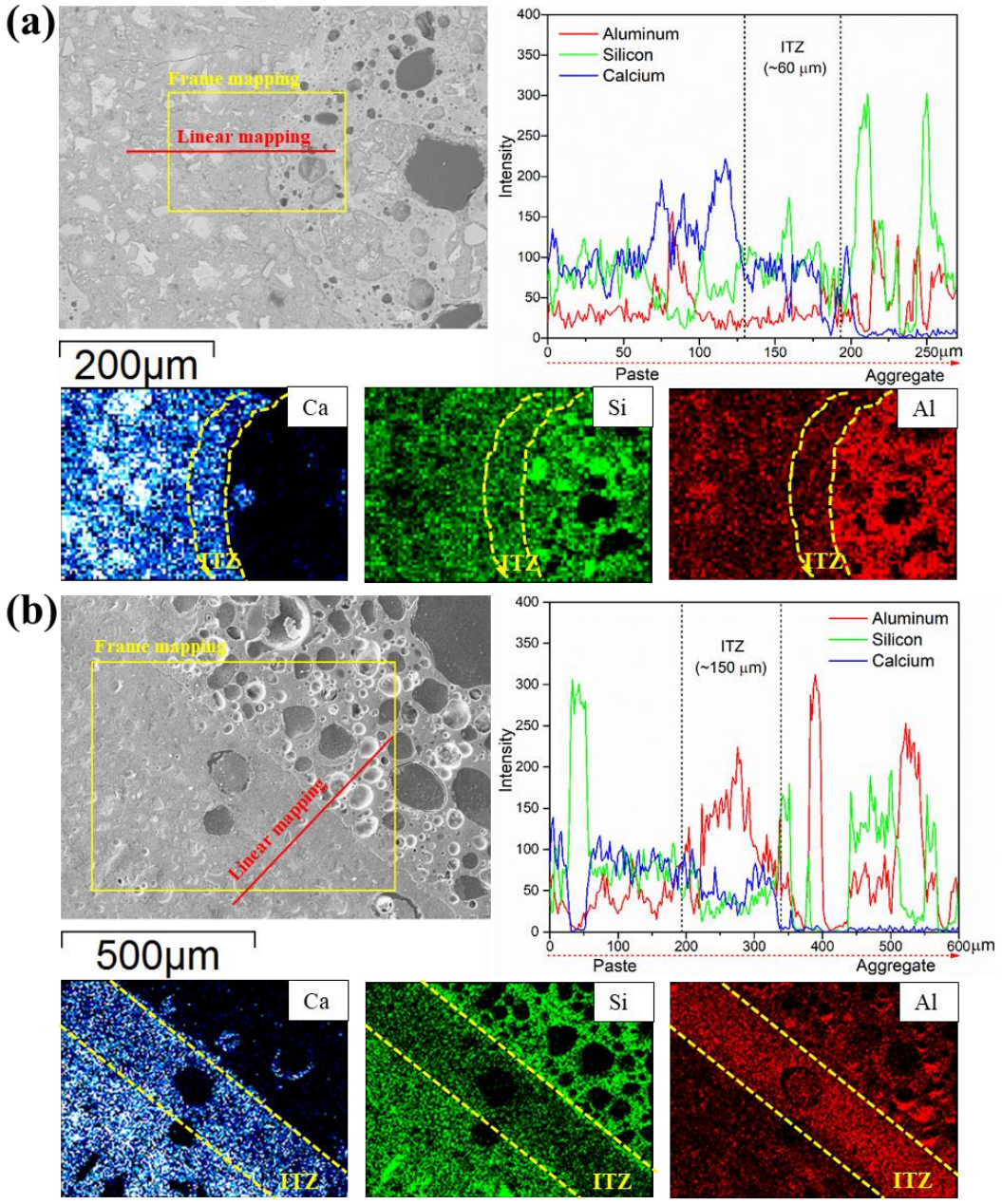

Fig. 14. Elemental mapping of ITZ, (a)100C and (b)100S.

3.3.3 Micromechanical properties of ITZ

The nanoindentation technique was used to explore the micromechanical properties in the ITZ. The ITZ boundary was demarcated by optical microscopy images and indentation matrices (Fig. 3). Fig. 15 shows the contour maps of micro-hardness and modulus of ITZ in the 100R, 100C, and 100S samples. The RS had a much higher hardness and modulus as compared to the bulk-paste,

660 thus the ITZ could be easily identified. Also, some unreacted clinker particles with high moduli
661 were found in the paste. It should be noted that a distinctive ITZ with a lower hardness and modulus
662 was present between the RS and the paste because the wall effect of the RS might increase the
663 local *w*/*b* ratio of the paste near the RS. The LWAs and the paste can be identified according to the
664 indentation images and the contour maps. The LWAs had a very low hardness and modulus since
665 they contained many pores. However, the ITZ around the LWAs seemed to have a higher hardness
666 and modulus.
667

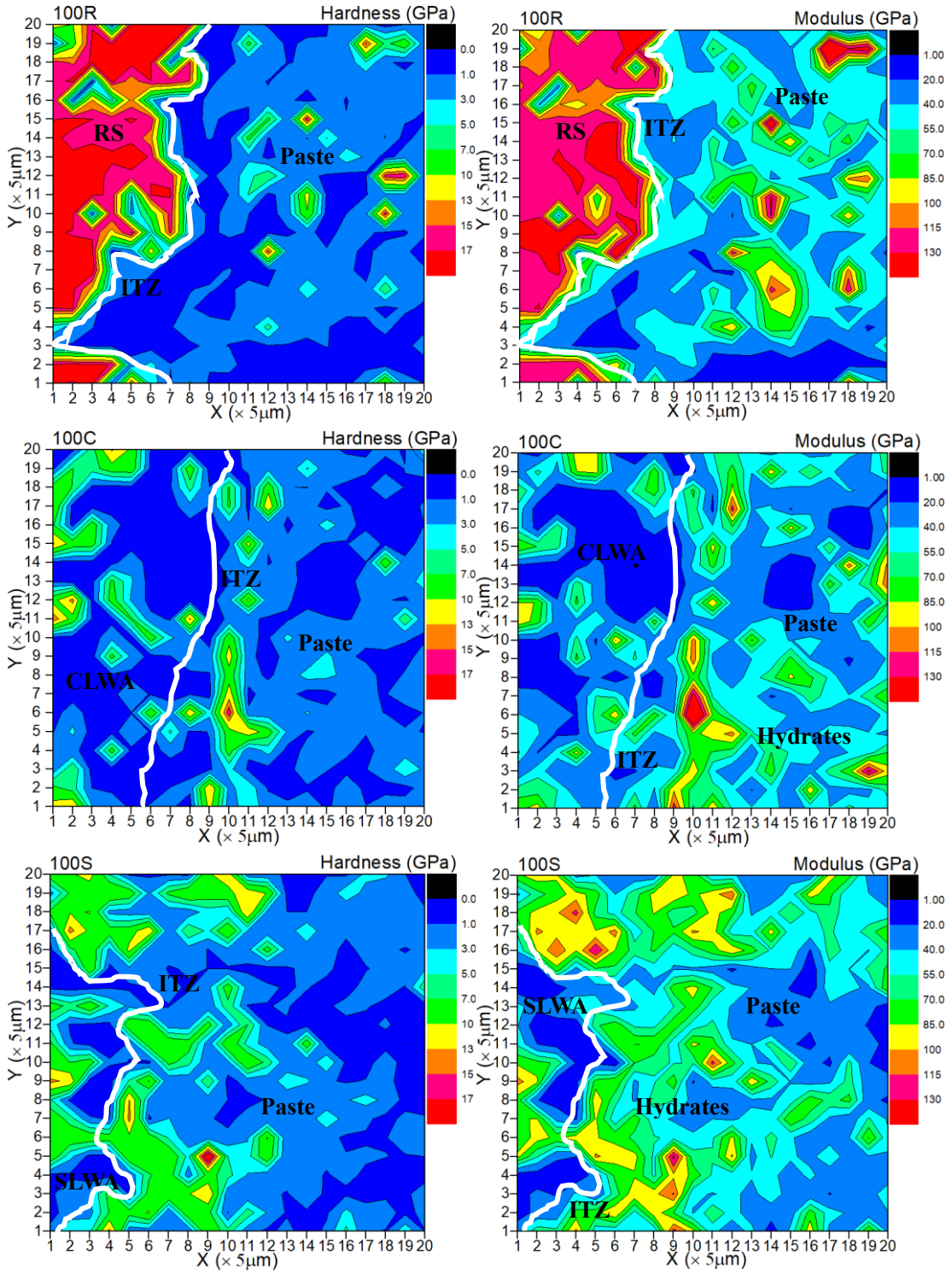

Fig. 15. Contour maps of micromechanical properties of ITZ in 100R, 100C and 100S.

668

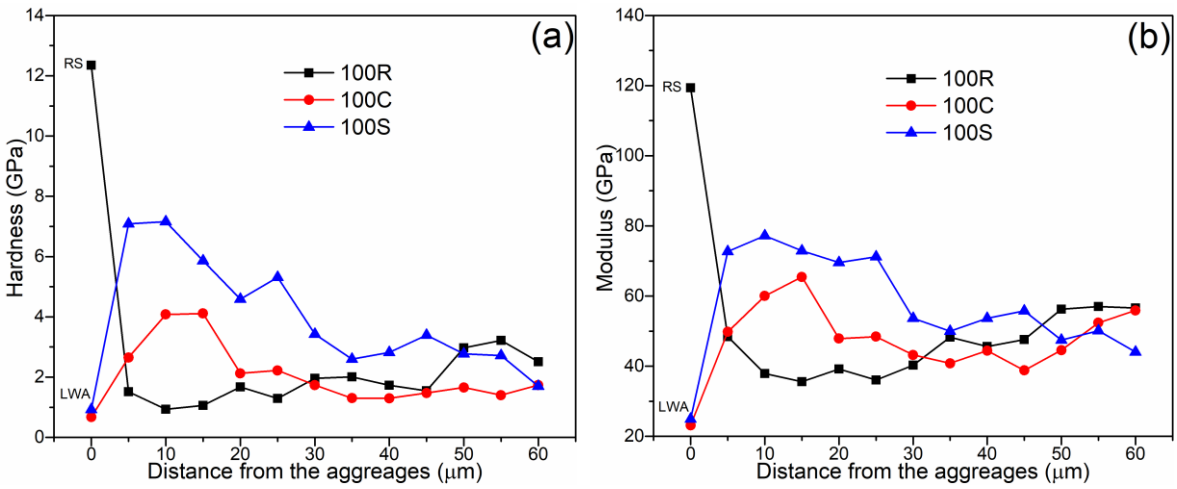

Fig. 16. Micromechanical properties of ITZ, (a) Hardness and (b) Modulus.

To quantitatively understand the evolution of the micromechanical properties in the ITZ, the average hardness and modulus values were plotted against the distance from the aggregates (to 60 μm) in Fig 16. For the 100R sample, both the hardness and modulus dropped sharply in the ITZ and then increased gradually with the increasing distance away from the RS. On the contrary, for the samples prepared with LWAs, the hardness and modulus values at the regions adjacent to the aggregates were higher than that of the aggregate, followed by a decreasing trend reaching a stable value. Thereinto, the ITZ between the SLWA and the paste exhibited better micromechanical performance than that of the CLWA and the paste. These results suggest that the incorporations of the LWAs were beneficial to improving the micromechanical properties of the ITZ in the UHPC matrix, and the improvement derived from the SLWA was more apparent than the CLWA. The enhancement of micromechanical properties of the ITZ was also reported in conventional concrete prepared with LWAs [106, 107]. Zhang et al. [107] attributed the higher micromechanical properties of ITZ to the higher amount of CH at the surface of LWAs. However, in this study, due to the use of UHPC paste with a very low *w*/*b* ratio, dense ITZ was formed and no crystalline products were deposited in the vicinity of LWAs. Hence, the improved ITZ of both cases was probably resulted from the internal curing of the pre-soaked LWAs, especially for the UHPC system, the water desorption from the LWAs reacted with the unhydrated cement to strengthen the ITZ around the LWAs. This enhancement would, to some extent, counteract the negative influence of the porous LWAs. For the sample prepared with SLWA, the higher pozzolanic activity of the SLWA further densified the ITZ, resulting in a higher micromechanical performance of ITZ. This

explanation is supported by the formation of additional C-A-S-H in the ITZ. Although the ITZ was strengthened by the internal curing and pozzolanic reaction of the LWAs, the compressive strength of overall concrete was still controlled by the weak strength of the LWAs. However, the better micromechanical performance of ITZ in the SLWA mixture as compared to that in the CLWA mixture might partly contribute to the higher compressive strength of the former. Moreover, the ref. [106] reported that the improved ITZ around SLWA could enhance the resistance of concrete to the ingress of harmful ions penetration. In the LWA concrete, the porous aggregate would be the weakest part when the concrete is subject to loading stress or harsh environment. Therefore, the strengthened ITZ was expected to prevent the loading cracks or defense the intrusion of harmful ions.

It is noted that the average modulus of C-S-H hydrate in this study was higher than 35 GPa, which was much higher than that in other works [108, 109]. This is because of the presence of a new hydration product (ultra high density C-S-H) in the matrix, formed with a low *w*/*b* ratio [110], in addition to the low density and high density C-S-H phases normally found in hydrated cement pastes. Furthermore, in the UHPC matrix, the high density and ultra high density C-S-H phases dominated the microstructure [110, 111]. Hence, the presence of the ultra high density C-S-H is believed to increase the modulus of the paste matrix. With the incorporation of the LWAs, the mean modulus of the ITZ was further increased due to the increased formation of C-S-H gels in the limited space, which would increase the packing and stiffness of hydrate phases. Similarly, in conventional lightweight aggregate concrete, other studies [112, 113] also reported that the microhardness of the ITZ around the LWAs was higher than the surrounding matrix as the newly formed product densified the interface structure. The improved micromechanical properties of the ITZ might contribute to the enhanced mechanical properties and durability of HPLACs.

3.3.4 Pore structure of paste

The pore size distributions of the paste matrices in the reference sample and HPLACs are plotted in Fig. 17. It should be noted that the pores of the LWAs in the samples have been excluded via testing the LWAs alone. Fig. 17a shows that most of the pores in the reference paste ranged from 5 to 100 nm, and by contrast, the pores in the 100C and 100S pastes were mainly concentrated in a smaller-size range (＜10 nm), which can be referred as gel pores [114]. As the gel pores are the

intrinsic porosity of the calcium silicate hydrate phase [66], the increased volume of gel pores is likely to indicate the increased hydration degree of the matrix. In this study, the internal curing of LWAs is considered to play a positive role in promoting the hydration of the UHPC matrix, thus increasing the amount of finer pores. These results are consistent with the enhanced hydration kinetic in the presence of the LWAs. A similar phenomenon was observed in the study of Liu and Wei [115], that the use of pre-wetted calcined bauxite LWAs resulted in increased amounts of gel pores and large capillary pores. Also, the amount of 10-50 nm capillary pores was found to be increased with the incorporation of the LWAs. This might be due to the water released from the LWAs at a very early age (or during the mixing) increased the water content in the paste. However, this range of mesopores has been regarded as less harmful pores, which means that they have less influence in affecting the strength and permeability of concrete [116]. The cumulative pore volume plotted in Fig. 17b shows the larger total pore volume in the pastes of the samples prepared with LWAs, which is primarily due to the larger amount of gel pores.

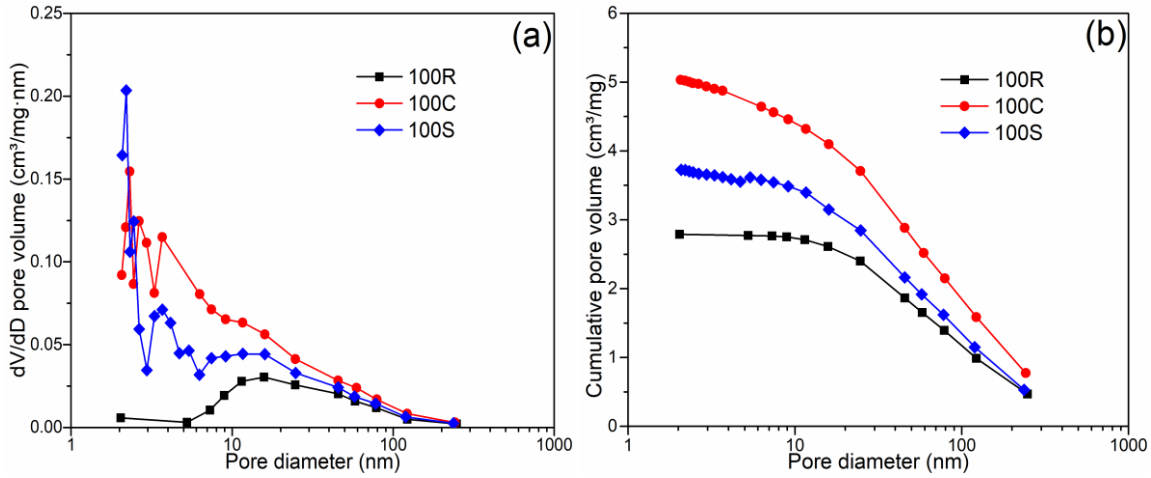

Fig. 17. Pore structure of paste in 100R, 100C and 100S determined by BET method.

4 Discussion

4.1 Judicious selection of LWAs based on their physicochemical properties

Besides the cement paste, the physicochemical properties of LWAs also played essential roles in affecting the performance of lightweight aggregate concrete [99]. Based on the characteristics of the LWAs and the corresponding performance of HPLACs in this study, several principles are proposed as selection criteria of LWAs for the preparation of HPLACs:

i) To make sure the HPLAC has high strength, a high-strength LWA is necessary to be adopted. Although the two types of LWAs had similar density and porosity, the SLWA had much higher strength than the CLWA (4.58 MPa vs. 0.76 MPa in Table 2), which partly contributed to the higher strength and structural efficiency of HPLACs. The strength of LWAs was associated with their pore structure [117]. As indicated by X-ray μCT observation (Fig. 18), the presence of relatively small, uniform, and isolated pores in the SLWA might account for its higher strength in comparison with the CLWA with a heterogeneous pore structure. This result is consistent with the finding of MIP (see Fig. 5), the different pore size distributions in two types of LWAs were expected to affect the absorption and desorption of water and further influence the internal curing effect of pre-wetted LWAs.

ii) The geometry of the LWAs affects the bonding of aggregates and paste (Fig. 2) and the open-pore surface of the SLWA (Figs. 6 and 7) was beneficial to improving the mechanical bonding between the aggregates and the paste [74]. Hence, the interlocking interface of the SLWA and matrix was able to strengthen the ITZ since the porous surface increased the bonding area as shown in SEM-BSE images (Section 3.3.2). Although the ITZ became better due to the internal curing and interlocking bonding of the LWAs, the compressive strength of HPLAC was still governed by the weak strength of the LWAs. Nonetheless, in comparison with the CLWA, the improved ITZ in the SLWA mixture was expected to result in a higher compressive strength (Section 3.3.3).

iii) An LWA which possesses a higher pozzolanic reactivity is preferred. As indicated by Q-XRD results (see Table 4), the SLWA had a higher content of amorphous phases than the CLWA. In combination with the composition of the LWAs, the amorphous silica and aluminate phases may be the major components in the LWAs, thus the larger amorphous amount tended to induce a higher pozzolanic reactivity. This speculation was confirmed by the Chapelle test in Fig. 8, which showed that the SLWA had a higher pozzolanic reactivity than the CLWA). Therefore, the chemical interaction between the SLWA and the paste was more pronounced. The reinforced reaction around the surface of the SLWA enhanced the micromechanical properties of ITZ, which would be able to counteract the weak strength of SLWA.

iv) An LWA with high open porosity is conducive to providing an internal curing effect by desorbing sufficient water. Especially for the UHPC system, the lack of water for cement hydration would make the cement superfluous. Thus, the incorporation of water-absorbing LWAs could promote the hydration of cement and the pozzolanic reaction of SCMs in the

HPLACs (Section 3.3.1). As shown in Table 2, the LWAs used in this study had high open porosity and large absorption capacity, hence the internal curing effect further benefited the pozzolanic reactivity of LWAs and the physicochemical reaction in the ITZ. However, it should be noted that LWAs with too large or too small pores are not endeared as the water inside would migrate out too early to increase the *w*/*b* ratio of the UHPC matrix, or cannot migrate out to play the internal curing role [118].

v) In order to produce high performance lightweight concrete, an LWA with low density or high total porosity is favorable to be used. In this study, two types of LWAs with low bulk density (about 500 kg/m^3 in Table 2) were selected to reduce the weight of concrete as much as possible (Fig. 9). Correspondingly, the thermal insulation of the LWAs-containing HPLACs was significantly reduced (see Fig. 11) due to the high porosity of the LWAs. In terms of physical and functional properties, if the content of LWAs exceeded 100%, the reductions in the density and the thermal conductivity tended to be less significant. Hence, to ensure high structural efficiency of concrete, 100% replacement of RS by the LWAs in the UHPC system seemed to be appropriate in the production of HPLACs.

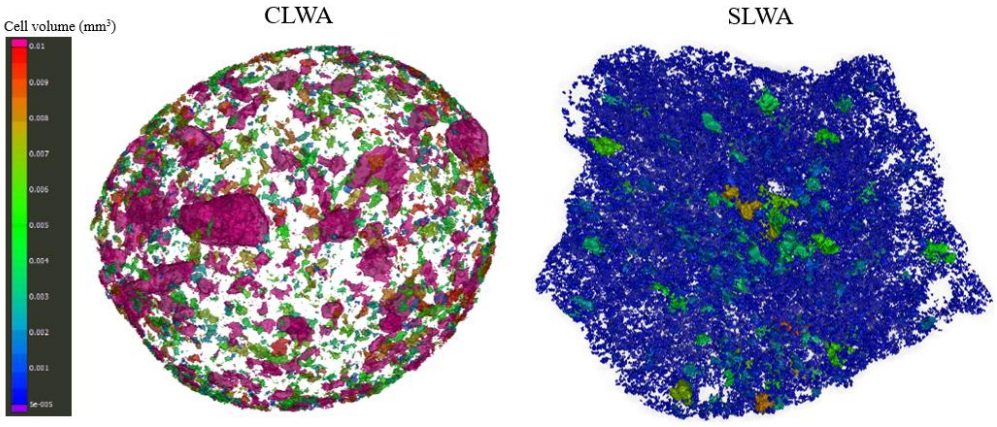

Fig. 18. 3D pore structures of CLWA and SLWA obtained by X-ray μCT.

Based on the above principles and performance of HPLACs, compared to CLWA, SLWA was more favorable to be used in the production of HPLACs with achieving higher structural efficiency. Thus, the interaction between the UHPC and the SLWA will be discussed in the following part.

4.2 Synergetic effects of UHPC and pre-soaked SLWA

4.2.1 Homogeneity of SLWA and fibers

One major concern of using LWAs in concrete is that the lightweight aggregate concrete is susceptible to segregation because of the lower density of LWAs [119]. However, the advantage of using the UHPC system is to mitigate the potential segregation of LWAs and fibers in the HPLAC. X-ray μCT was employed to observe the distributions of aggregates in the 100R and 100S. As seen in Fig. 19, the distributions of RS and SLWA were homogeneous and the heavy steel fibers did not sink to the bottom or agglomerate at one site in the HPLAC. The good homogeneity is because the fresh UHPC paste had a high viscosity [120], which increased the adhesion between LWAs/fibers and the matrix. Hence, the use of UHPC was beneficial to the homogeneity of LWAs and fibers in the HPLAC.

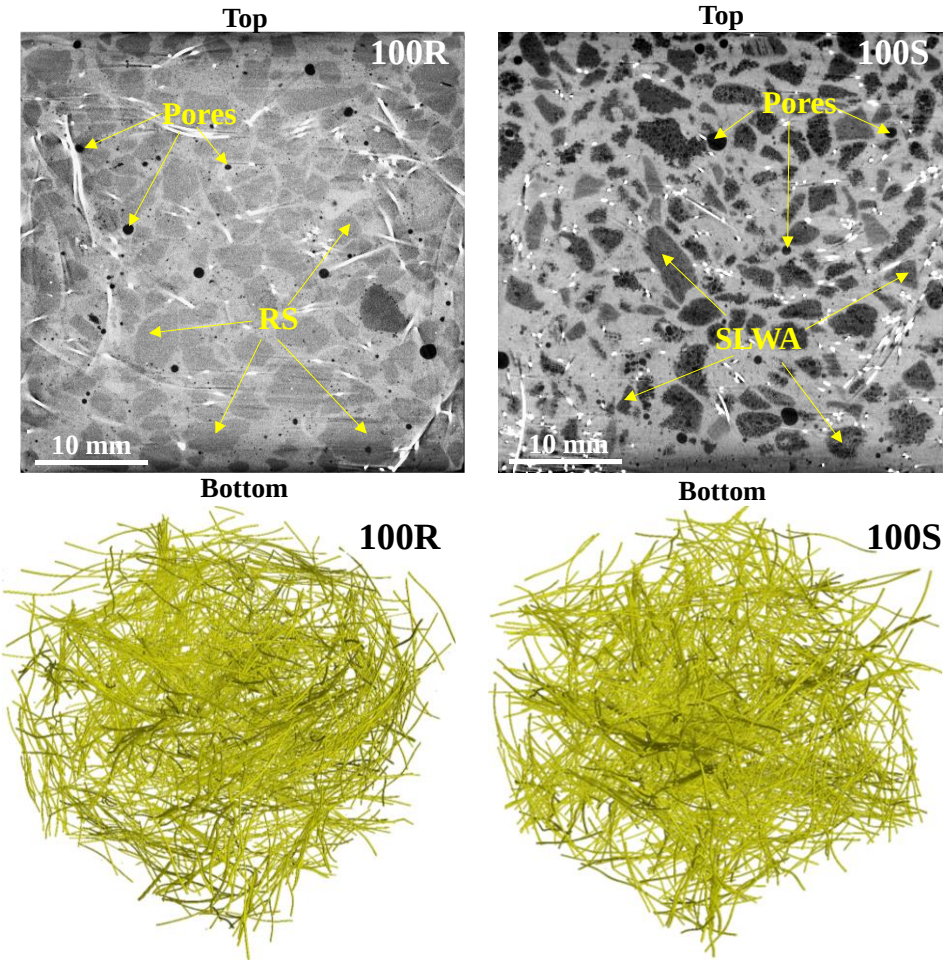

Fig. 19. 2D vertical-section images (right view) and 3D distributions of steel fibers (top-right-back view) in 100R and 100S obtained by X-ray μCT.

4.2.2 Durability of HPLAC

To prepare a HPLAC, a good quality cement paste is needed. Hence, an UHPC was applied as the binder in this study due to its excellent mechanical and durability properties. Zhang and Gjørv [44] pointed out that the permeability of lightweight aggregate concrete was mainly controlled by the porosity of cement paste/mortar rather than the porous aggregates. The low porosity and fine pores characteristics of the UHPC have been proven due to its extremely low *w*/*b* ratio and the presence of a large amount of highly reactive powder [121, 122]. Therefore, the utilization of UHPC to bind the LWAs can provide a strong skeleton for the concrete and further protect the LWAs to resist the infiltration of aggressive substances. Fig. 20a shows the chloride ion penetration values for the reference UHPC and HPLAC prepared with SLWA. The results indicate that the 100S had a slightly higher charge passing value than the 100R, but both of them were much lower than the stipulated limit of "very low ion penetrability" [63]. Also, the ability of 100S to resist chloride ingress was better than conventional high strength HPLAC [123, 124] and comparable or superior to high performance concrete [125, 126]. The very low water absorption of the SLWA samples (Section 3.2.1) further confirmed the high resistance to external substance. Therefore, it can be concluded that the combined use of the UHPC and the SLWA can produce an HPLAC with low permeability. Besides the contribution from the UHPC paste, the released water from the SLWA enhanced the hydration degree of the UHPC, which contributed to the improvement of ITZ surrounding the SLWA by mechanical interlocking and chemical interaction (pozzolanic reaction). This might be another reason for the high resistance to chloride penetration and low water absorption.

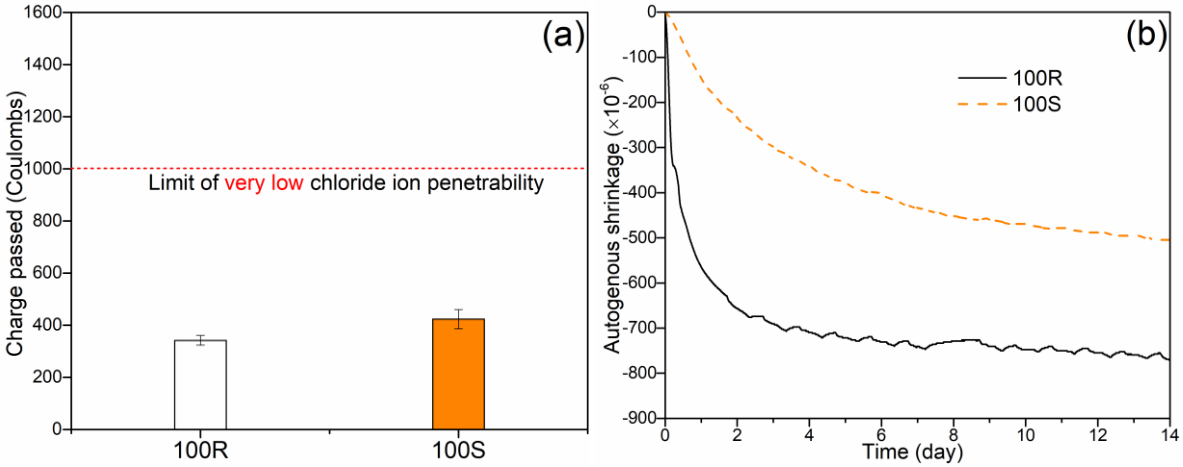

Fig. 20. Permeability (a) and autogenous shrinkage (b) of 100R and 100S.

It is known that one major concern of UHPC-based matrix is its high shrinkage (mainly autogenous shrinkage) due to the use of low *w*/*b* ratios, a large amount of SCMs, and the absence of coarse aggregates [127, 128]. The internal curing provided by the pre-wetted LWAs had been proven to successfully mitigate the autogenous shrinkage of conventional cement concrete [47, 129]. In recent years, some investigations [130-132] also found that the use of pre-wetted LWAs could reduce the autogenous shrinkage of UHPC. Therefore, a similar effect resulting from pre-soaked SLWA is believed to reduce the autogenous shrinkage of the HPLACs since more LWAs were incorporated. As shown in Fig. 20b, the HPLAC prepared with 100% SLWA had a much lower autogenous shrinkage value than the reference UHPC within 14 days. It can be noted that the most of autogenous shrinkage occurred at the very early age (within 24 h) for the reference UHPC. Shen et al. [130] found that the internal humidity of UHPC was nearly saturated within 48 h by incorporating a certain amount of LWAs. Therefore, the water desorbed from the SLWA mitigated the self-desiccation of the UHPC matrix (withdrawal of water from capillary pores) by increasing the internal moisture [87], and thus reducing the autogenous shrinkage of the HPLACs.

As the LWAs had a higher reactivity than the quartz sand (Section 3.1.3), alkali-silica-reaction (ASR) may be one concern in the conventional LWA concrete. However, in this study, the ASR would not be triggered after taking several factors into account: 1) Due to the large amounts of pozzolanic materials in the mixture (i.e. SF, MK and GGBS), the ASR would be suppressed by these SCMs [133]. 2) As the LWAs were porous, the internal pores were expected to accommodate the expansion stress if ASR would occur. 3) Lack of water for the ASR reaction in the system because of the low *w*/*b* ratio. A recent study [98] also indicated that the expanded clay and shale showed superiority in limiting the ASR expansion by the reduction of alkalinity and release of Al in pore solution.

4.2.3 Interaction of UHPC and SLWA

The physical and chemical characteristics of LWAs influenced the overall performance of lightweight aggregate concrete by processes that took place in the ITZ [99]. A schematic illustration of the mechanisms of interactions between the UHPC and the pre-soaked SLWA is illustrated in Fig. 21. In the fresh stage, the cement paste penetrated into the cavities/pores on the SLWA surface, which created a better interface bonding. This interlocking bonding of the SLWA is similar to other LWAs, such as porous calcined bauxite [134] and porous pumice [131]. During

the hardening stage, the internal curing of the SLWA provided additional water to further hydrate the remaining cement clinkers and the pozzolanic reaction of SCMs. Moreover, a high concentration of Al was leached out from the SLWA and involved in the reaction to form C-A-S-H hydrates. The formation of C-A-S-H in the ITZ was also an evidence of the occurrence of pozzolanic activity of the SLWA. As a result, with the progress of hydration, the interaction of the SLWA and the alkaline products formed a pozzolanic product layer in the vicinity of the SLWA [71], which further strengthened the ITZ. The synergetic effects of the above reactions led to the formation of a dense rim with higher micromechanical properties in the ITZ, which protected the porous aggregates against the penetration of the detrimental ions [44]. Due to the presence of the UHPC matrix and coupled effects of internal curing and the pozzolanic reaction of the SLWA, an HPLAC with high structural efficiency and good durability was produced with the use of UHPC and pre-wetted SLWA together.

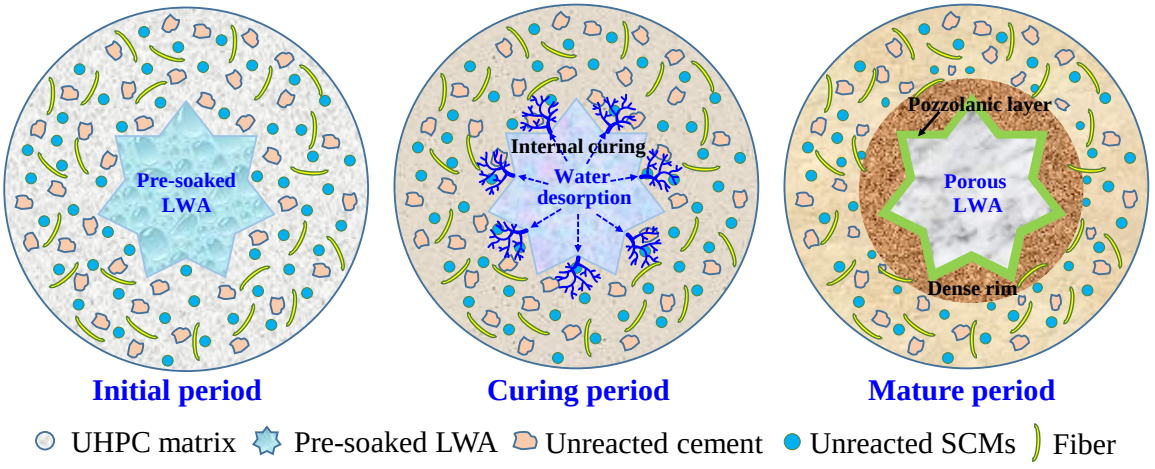

Fig. 21. Schematic illustration of interaction of SLWA and UHPC in the HPLACs.

5 Conclusion

In this study, a high performance lightweight aggregate concrete (HPLAC) was developed by combining the use of UHPC and LWAs. The role of physicochemical properties of two types of LWAs in the HPLACs was investigated with a view to selecting the optimal LWAs. The effectiveness of the combined use of the UHPC and the LWAs in affecting the physical, functional, and permeability properties was evaluated and analyzed. The physical and chemical interfacial processes between the UHPC and the LWAs were discussed in light of hydration kinetic, nanoindentation, elemental mapping, and X-ray μCT measurements. The following conclusions

889 can be derived from this study:
890
891 (I) The shale based LWA (SLWA) exhibited a higher pozzolanic reactivity than the clay based
892 LWA (CLWA) attributed to the higher content of amorphous phase and lower quartz content
893 in the SLWA. The SLWA had an open pores surface and a more individual and fine pore
894 structure, while the CLWA had a relatively denser outer shell and well-interconnected coarser
895 pores.

896 (II) The incorporation of the two types of LWAs reduced the density of HPLACs significantly.
897 However, the reductions in the density using the CLWA and the SLWA were similar due to
898 their similar wet density values. The water absorption values of HPLACs were much lower
899 than those of conventional LWA concrete and normal weight concrete. The SLWA-
900 incorporated HPLACs had lower water absorption than the CLWA-containing samples.

901 (III) The HPLACs prepared with SLWA exhibited a higher structural efficiency than the CLWA-
902 incorporated HPLACs due to the higher strength of the SLWA, improved interlocking
903 bonding of aggregates and paste, higher pozzolanic reactivity of the SLWA. The replacement
904 of RS by the two types of LWAs in the HPLACs effectively reduced the thermal conductivity.

905 (IV) The internal curing of the pre-wetted LWAs promoted the hydration of the cementitious
906 materials in the UHPC system due to the water desorption characteristics of the LWAs. The
907 internal curing effect of the pre-wetted SLWA was more pronounced than that of the CLWA.
908 Higher intensity of Al and lower intensities of Si and Ca in the ITZ were found in the SLWA-
909 incorporated sample. Due to the pozzolanic reaction and internal curing of the SLWA, C-A-
910 S-H hydrates with a lower Ca/(Si+Al) ratio were formed in the vicinity of the SLWA. The
911 use of the LWAs in the UHPC matrix improved the micromechanical properties of the ITZ,
912 and the improvement resulted from the SLWA was more significant than the CLWA because
913 of the coupled effects of the higher pozzolanic reaction and internal curing of the SLWA.

914 (V) The preferred characteristics of the LWAs to be used for producing HPLAC are: high
915 strength with a low density, high porosity with a fine pore structure, a porous surface, and
916 high pozzolanic reactivity. The use of UHPC was beneficial to the homogeneity of the LWAs
917 and fibers in the HPLACs. The conjunct use of the UHPC and the SLWA was able to produce

an HPLAC with high structural efficiency, low autogenous shrinkage, good thermal insulation, and low permeability.

Acknowledgment

The authors wish to thank the financial support from the Hong Kong Polytechnic University. Mr. Lu would like to appreciate the Teaching Postgraduate Studentship Scheme. The technical assistance of Ms. Dorothy Chan in conducting the MIP and BET tests are gratefully acknowledged. Thanks are also due to Dr. Ting Fai Kong (Department of Industrial and Systems Engineering) for his help in performing the micro-CT experiment.

References

[1] Hong Kong Construction Industry Council (CIC), About MiC, http://www.cic.hk/eng/main/mic/whatsmic/aboutmic/, (2020).
[2] W. Zhang, M.W. Lee, L. Jaillon, C.-S. Poon, The hindrance to using prefabrication in Hong Kong's building industry, Journal of Cleaner Production, 204 (2018) 70-81.
[3] S. Abdelmageed, T. Zayed, A study of literature in modular integrated construction - Critical review and future directions, Journal of Cleaner Production, 277 (2020) 124044.
[4] W. Ferdous, Y. Bai, T.D. Ngo, A. Manalo, P. Mendis, New advancements, challenges and opportunities of multi-storey modular buildings – A state-of-the-art review, Engineering Structures, 183 (2019) 883-893.
[5] BS EN 206+A1, Concrete — Specification, performance, production and conformity, British Standard Institution, (2016).
[6] ACI 213R-03, Guide for structural lightweight-aggregate concrete, American Concrete Institute, (2003).
[7] J. Mena, M. González, J.C. Remesar, M. Lopez, Developing a very high-strength low-CO_2 cementitious matrix based on a multi-binder approach for structural lightweight aggregate concrete, Construction and Building Materials, 234 (2020) 117830.
[8] J.-X. Lu, P. Shen, H. Zheng, H.A. Ali, C.S. Poon, Development and characteristics of ultra high-performance lightweight cementitious composites (UHP-LCCs), Cement and Concrete Research, 145 (2021) 106462.
[9] K.S. Chia, M.-H. Zhang, Water permeability and chloride penetrability of high-strength lightweight aggregate concrete, Cement and Concrete Research 32 (2002) 639–645.
[10] D.W. Mitchell, H. Marzouk, Bond characteristics of high-strength lightweight concrete, ACI Structural Journal, 104 (2007).
[11] E.G. Moffatt, M.D.A. Thomas, Performance of 25-year-old silica fume and fly ash lightweight concrete blocks in a harsh marine environment, Cement and Concrete Research, 113 (2018) 65-73.
[12] M. Thomas, T. Bremner, Performance of lightweight aggregate concrete containing slag after 25years in a harsh marine environment, Cement and Concrete Research, 42 (2012) 358-364.
[13] M.S. Nadesan, P. Dinakar, Influence of type of binder on high-performance sintered fly ash lightweight aggregate concrete, Construction and Building Materials, 176 (2018) 665-675.
[14] B. Chen, J. Liu, Experimental application of mineral admixtures in lightweight concrete with high strength and workability, Construction and Building Materials, 22 (2008) 1108-1113.
[15] A. Kılıç, C.D. Atiş, E. Yaşar, F. Özcan, High-strength lightweight concrete made with scoria aggregate containing mineral admixtures, Cement and Concrete Research, 33 (2003) 1595-1599.
[16] H. S. Wilson, V.M. Malhotra, Development of high strength lightweight concrete for structural applications, International Journal of Cement Composites & Lightwght Concrete, 10 (1988) 79-90.
[17] P. Seabrook, H. Wilson, High strength lightweight concrete for use in offshore structures: utilisation of fly ash

962 and silica fume, International Journal of Cement Composites and Lightweight Concrete, 10 (1988) 183-192.
963 [18] N. Atmaca, M.L. Abbas, A. Atmaca, Effects of nano-silica on the gas permeability, durability and mechanical
964 properties of high-strength lightweight concrete, Construction and Building Materials, 147 (2017) 17-26.
965 [19] D. Moreno, F. Zunino, Á. Paul, M. Lopez, High strength lightweight concrete (HSLC): Challenges when moving
966 from the laboratory to the field, Construction and Building Materials, 56 (2014) 44-52.
967 [20] S. Real, J.A. Bogas, Oxygen permeability of structural lightweight aggregate concrete, Construction and Building
968 Materials, 137 (2017) 21-34.
969 [21] S. Real, J.A. Bogas, J. Pontes, Chloride migration in structural lightweight aggregate concrete produced with
970 different binders, Construction and Building Materials, 98 (2015) 425-436.
971 [22] N.U. Kockal, T. Ozturan, Optimization of properties of fly ash aggregates for high-strength lightweight concrete
972 production, Materials & Design, 32 (2011) 3586-3593.
973 [23] N.U. Kockal, T. Ozturan, Strength and elastic properties of structural lightweight concretes, Materials & Design,
974 32 (2011) 2396-2403.
975 [24] M. Lopez, L.F. Kahn, K.E. Kurtis, Characterization of elastic and time-dependent deformations in high
976 performance lightweight concrete by image analysis, Cement and Concrete Research, 39 (2009) 610-619.
977 [25] X. Liu, K.S. Chia, M.-H. Zhang, Water absorption, permeability, and resistance to chloride-ion penetration of
978 lightweight aggregate concrete, Construction and Building Materials, 25 (2011) 335–343.
979 [26] J.A. Rossignolo, M.V.C. Agnesini, J.A. Morais, Properties of high-performance LWAC for precast structures with
980 brazilian lightweight aggregates, Cement & Concrete Composites, 25 (2003) 77-82.
981 [27] M. Osman, H. Marzouk, S. Helmy, Behavior of high-strength lightweight concrete slabs under punching loads,
982 ACI Structural Journal, 97 (2000).
983 [28] M. Aslam, P. Shafigh, M. Alizadeh Nomeli, M. Zamin Jumaat, Manufacturing of high-strength lightweight
984 aggregate concrete using blended coarse lightweight aggregates, Journal of Building Engineering, 13 (2017) 53-62.
985 [29] R. Ahmmad, M.Z. Jumaat, U.J. Alengaram, S. Bahri, M.A. Rehman, H.b. Hashim, Performance evaluation of
986 palm oil clinker as coarse aggregate in high strength lightweight concrete, Journal of Cleaner Production, 112 (2016)
987 566-574.
988 [30] P. Shafigh, M.Z. Jumaat, H.B. Mahmud, U.J. Alengaram, A new method of producing high strength oil palm shell
989 lightweight concrete, Materials & Design, 32 (2011) 4839-4843.
990 [31] M. Smadi, E. Migdady, Properties of high strength tuff lightweight aggregate concrete, Cement and Concrete
991 Composites, 13 (1991) 129-135.
992 [32] J.A. Bogas, A. Carriço, J. Pontes, Influence of cracking on the capillary absorption and carbonation of structural
993 lightweight aggregate concrete, Cement and Concrete Composites, 104 (2019) 103382.
994 [33] J.C. Remesar, S. Vera, M. Lopez, Assessing and understanding the interaction between mechanical and thermal
995 properties in concrete for developing a structural and insulating material, Construction and Building Materials, 132
996 (2017) 353-364.
997 [34] R. Le Roy, E. Parant, C. Boulay, Taking into account the inclusions' size in lightweight concrete compressive
998 strength prediction, Cement and Concrete Research, 35 (2005) 770-775.
999 [35] A.F. Angelin, R.C. Cecche Lintz, W.R. Osório, L.A. Gachet, Evaluation of efficiency factor of a self-compacting
1000 lightweight concrete with rubber and expanded clay contents, Construction and Building Materials, 257 (2020) 119573.
1001 [36] C. Pla, A.J. Tenza-Abril, J. Valdes-Abellan, D. Benavente, Influence of microstructure on fluid transport and
1002 mechanical properties in structural concrete produced with lightweight clay aggregates, Construction and Building
1003 Materials, 171 (2018) 388-396.
1004 [37] H. Al-Khaiat, N. Haque, Strength and durability of lightweight and normal weight concrete, Journal of Materials
1005 in Civil Engineering, 11 (1999).
1006 [38] J.A. Bogas, R. Nogueira, N.G. Almeida, Influence of mineral additions and different compositional parameters
1007 on the shrinkage of structural expanded clay lightweight concrete, Materials & Design (1980-2015), 56 (2014) 1039-
1008 1048.
1009 [39] J. Li, J. Niu, C. Wan, X. Liu, Z. Jin, Comparison of flexural property between high performance polypropylene
1010 fiber reinforced lightweight aggregate concrete and steel fiber reinforced lightweight aggregate concrete, Construction
1011 and Building Materials, 157 (2017) 729-736.
1012 [40] S. Iqbal, A. Ali, K. Holschemacher, T.A. Bier, Mechanical properties of steel fiber reinforced high strength
1013 lightweight self-compacting concrete (SHLSCC), Construction and Building Materials, 98 (2015) 325-333.
1014 [41] J. Gao, W. Sun, K. Morino, Mechanical properties of steel fiber-reinforced, high-strength, lightweight concrete,
1015 Cement and Concrete Composites, 19 (1997) 307-313.
1016 [42] O. Kayali, M. Haque, B. Zhu, Some characteristics of high strength fiber reinforced lightweight aggregate
1017 concrete, Cement and Concrete Composites, 25 (2003) 207-213.

[43] M.-H. Zhang, L. Li, P. Paramasivam, Shrinkage of high-strength lightweight aggregate concrete exposed to dry environment, ACI Materials Journal, 102 (2005) 86-92.
[44] M.-H. Zhang, O.E. Gjørv, Permeability of high-strength lightweight concrete, ACI Material Journal, 88 (1991) 463-469.
[45] M.C.S. Nepomuceno, L.A. Pereira-de-Oliveira, S.F. Pereira, Mix design of structural lightweight self-compacting concrete incorporating coarse lightweight expanded clay aggregates, Construction and Building Materials, 166 (2018) 373-385.
[46] W. Meng, K. Khayat, Effects of saturated lightweight sand content on key characteristics of ultra-high-performance concrete, Cement and Concrete Research, 101 (2017) 46-54.
[47] R. Henkensiefken, D. Bentz, T. Nantung, J. Weiss, Volume change and cracking in internally cured mixtures made with saturated lightweight aggregate under sealed and unsealed conditions, Cement and Concrete Composites, 31 (2009) 427-437.
[48] D. Cusson, T. Hoogeveen, Internal curing of high-performance concrete with pre-soaked fine lightweight aggregate for prevention of autogenous shrinkage cracking, Cement and Concrete Research, 38 (2008) 757-765.
[49] M. Valipour, K.H. Khayat, Coupled effect of shrinkage-mitigating admixtures and saturated lightweight sand on shrinkage of UHPC for overlay applications, Construction and Building Materials, 184 (2018) 320-329.
[50] T. Deboodt, T. Fu, J.H. Ideker, Durability assessment of high-performance concrete with SRAs and FLWAs, Cement and Concrete Composites, 57 (2015) 94-101.
[51] S. Yashima, Y. Kanda, S. Sano, Relationships between particle size and fracture energy or impact velocity required to fracture as estimated from single particle crushing, Powder technology, 51 (1987) 277-282.
[52] C.R. Cheeseman, G.S. Virdi, Properties and microstructure of lightweight aggregate produced from sintered sewage sludge ash, Resources, Conservation and Recycling, 45 (2005) 18-30.
[53] M.-H. Zhang, O.E. Gjørv, Characteristics of lightweight aggregates for high-strength concrete, ACI Materials Journal, 88 (1991) 150-158.
[54] M. Wyrzykowski, S. Ghourchian, S. Sinthupinyo, N. Chitvoranund, T. Chintana, P. Lura, Internal curing of high performance mortars with bottom ash, Cement and Concrete Composites, 71 (2016) 1-9.
[55] X. Ma, J. Liu, C. Shi, A review on the use of LWA as an internal curing agent of high performance cement-based materials, Construction and Building Materials, 218 (2019) 385-393.
[56] BS EN 1015-3/A2, Methods of test for mortar for masonry - Part 3: Determination of consistence of fresh mortar (by flow table), British Standard Institution, (2007).
[57] H.A. Ali, D. Xuan, C.S. Poon, Assessment of long-term reactivity of initially lowly-reactive solid wastes as supplementary cementitious materials (SCMs), Construction and Building Materials, 232 (2020) 117192.
[58] R. Snellings, K.L. Scrivener, Rapid screening tests for supplementary cementitious materials: past and future, Materials and Structures, 49 (2015) 3265-3279.
[59] X. Li, R. Snellings, M. Antoni, N.M. Alderete, M. Ben Haha, S. Bishnoi, Ö. Cizer, M. Cyr, K. De Weerdt, Y. Dhandapani, J. Duchesne, J. Haufe, D. Hooton, M. Juenger, S. Kamali-Bernard, S. Kramar, M. Marroccoli, A.M. Joseph, A. Parashar, C. Patapy, J.L. Provis, S. Sabio, M. Santhanam, L. Steger, T. Sui, A. Telesca, A. Vollpracht, F. Vargas, B. Walkley, F. Winnefeld, G. Ye, M. Zajac, S. Zhang, K.L. Scrivener, Reactivity tests for supplementary cementitious materials: RILEM TC 267-TRM phase 1, Materials and Structures, 51 (2018).
[60] ASTM C109/C109M-20a, Standard test method for compressive strength of hydraulic cement mortars (Using 2-in. or [50-mm] cube specimens), American Society of Testing Materials, (2020).
[61] BS EN 12390-7, Testing hardened concrete Part 7: Density of hardened concrete, British Standard Institution, (2019).
[62] ASTM C642-13, Standard test method for density, absorption, and voids in hardened concrete, American Society of Testing Materials, (2013).
[63] ASTM C1202-19, Standard test method for electrical indication of concrete's ability to resist chloride ion penetration, American Society of Testing Materials, (2019).
[64] C. Shi, Effect of mixing proportions of concrete on its electrical conductivity and the rapid chloride permeability test (ASTM C1202 or ASSHTO T277) results, Cement and Concrete Research, 34 (2004) 537-545.
[65] ASTM C1698-19, Standard test method for autogenous strain of cement paste and mortar, American Society of Testing Materials, (2019).
[66] K. Scrivener, R. Snellings, B. Lothenbach, A practical guide to microtructral analysis of cementitious materials, CRC Press, New York, USA, (2016).
[67] F. Moro, H. Böhni, Ink-bottle effect in mercury intrusion porosimetry of cement-based materials, Journal of Colloid and Interface Science, 246 (2002) 135-149.
[68] G. Pharr, A. Bolshakov, Understanding nanoindentation unloading curves, Journal of Materials Research, 17

(2002) 2660-2671.
[69] W.C. Oliver, G.M. Pharr, An improved technique for determining hardness and elastic modulus using load and displacement sensing indentation experiments, Journal of Materials Research, 7 (1992) 1564-1583.
[70] M.-H. Zhang, O.E. Gjørv, Pozzolanic reactivity of lightweight aggregates, Cement and Concrete Research, 20 (1990) 884-890.
[71] S. Nie, S. Hu, F. Wang, C. Hu, X. Li, Y. Zhu, Pozzolanic reaction of lightweight fine aggregate and its influence on the hydration of cement, Construction and Building Materials, 153 (2017) 165-173.
[72] L. Kong, L. Hou, Y. Du, Chemical reactivity of lightweight aggregate in cement paste, Construction and Building Materials, 64 (2014) 22-27.
[73] M.-H. Zhang, O.E. Gjørv, Penetration of cement paste into lightweight aggregate, Cement and Concrete Research, 22 (1992) 47-55.
[74] M.-H. Zhang, O.E. Gjørv, Microstructure of the interfacial zone between lightweight aggregate and cement paste, Cement and Concrete Research, 20 (1990) 610-618.
[75] P. Suraneni, T. Fu, V. Jafari Azad, O.B. Isgor, J. Weiss, Pozzolanicity of finely ground lightweight aggregates, Cement and Concrete Composites, 88 (2018) 115-120.
[76] W. Tasong, J. Cripps, C. Lynsdale, Aggregate-cement chemical interactions, Cement and Concrete Research, 28 (1998) 1037-1048.
[77] T. Wu, X. Yang, H. Wei, X. Liu, Mechanical properties and microstructure of lightweight aggregate concrete with and without fibers, Construction and Building Materials, 199 (2019) 526-539.
[78] S. Ng, B.P. Jelle, L.I.C. Sandberg, T. Gao, Ó.H. Wallevik, Experimental investigations of aerogel-incorporated ultra-high performance concrete, Construction and Building Materials, 77 (2015) 307-316.
[79] Z. Kammoun, A. Trabelsi, A high-strength lightweight concrete made using straw, Magazine of Concrete Research, 72 (2020) 460-470.
[80] A. Dixit, S.D. Pang, S.-H. Kang, J. Moon, Lightweight structural cement composites with expanded polystyrene (EPS) for enhanced thermal insulation, Cement and Concrete Composites, 102 (2019) 185-197.
[81] İ.B. Topçu, T. Uygunoğlu, Effect of aggregate type on properties of hardened self-consolidating lightweight concrete (SCLC), Construction and Building Materials, 24 (2010) 1286-1295.
[82] M.L. Torres, P.A. García-Ruiz, Lightweight pozzolanic materials used in mortars: Evaluation of their influence on density, mechanical strength and water absorption, Cement and Concrete Composites, 31 (2009) 114-119.
[83] J. Castro, D. Bentz, J. Weiss, Effect of sample conditioning on the water absorption of concrete, Cement and Concrete Composites, 33 (2011) 805-813.
[84] R. Kurda, J. de Brito, J.D. Silvestre, Water absorption and electrical resistivity of concrete with recycled concrete aggregates and fly ash, Cement and Concrete Composites, 95 (2019) 169-182.
[85] D.S. Babu, K. Ganesh Babu, W. Tiong-Huan, Effect of polystyrene aggregate size on strength and moisture migration characteristics of lightweight concrete, Cement and Concrete Composites, 28 (2006) 520-527.
[86] K.-i. Horai, Thermal conductivity of rock-forming minerals, Journal of Geophysical Research, 76 (1971) 1278-1308.
[87] P. Shen, L. Lu, F. Wang, Y. He, S. Hu, J. Lu, H. Zheng, Water desorption characteristics of saturated lightweight fine aggregate in ultra-high performance concrete, Cement and Concrete Composites, 106 (2020) 103456.
[88] H. Oktay, R. Yumrutaş, A. Akpolat, Mechanical and thermophysical properties of lightweight aggregate concretes, Construction and Building Materials, 96 (2015) 217-225.
[89] S. Yang, T.-C. Ling, H. Cui, C.S. Poon, Influence of particle size of glass aggregates on the high temperature properties of dry-mix concrete blocks, Construction and Building Materials, 209 (2019) 522-531.
[90] P. Shen, H. Zheng, D. Xuan, J.-X. Lu, C.S. Poon, Feasible use of municipal solid waste incineration bottom ash in ultra-high performance concrete, Cement and Concrete Composites, 114 (2020).
[91] J.-X. Lu, C.S. Poon, Improvement of early-age properties for glass-cement mortar by adding nanosilica, Cement and Concrete Composites, 89 (2018) 18-30.
[92] J.W. Bullard, H.M. Jennings, R.A. Livingston, A. Nonat, G.W. Scherer, J.S. Schweitzer, K.L. Scrivener, J.J. Thomas, Mechanisms of cement hydration, Cement and Concrete Research, 41 (2011) 1208-1223.
[93] A. Quennoz, K.L. Scrivener, Hydration of C_3A–gypsum systems, Cement and Concrete Research, 42 (2012) 1032-1041.
[94] K.L. Scrivener, The development of microstructure during the hydration of portland cement, University of London, PhD Thesis, (1984).
[95] J.-X. Lu, Z.-H. Duan, C.S. Poon, Combined use of waste glass powder and cullet in architectural mortar, Cement and Concrete Composites, 82 (2017) 34-44.
[96] F. Lagier, K.E. Kurtis, Influence of Portland cement composition on early age reactions with metakaolin, Cement

and Concrete Research, 37 (2007) 1411-1417.
[97] J. Wei, B. Gencturk, Hydration of ternary Portland cement blends containing metakaolin and sodium bentonite, Cement and Concrete Research, 123 (2019) 105772.
[98] C. Li, M.D.A. Thomas, J.H. Ideker, A mechanistic study on mitigation of alkali-silica reaction by fine lightweight aggregates, Cement and Concrete Research, 104 (2018) 13-24.
[99] R. Wasserman, A. Bentur, Interfacial interactions in lightweight aggregate concretes and their influence on the concrete strength, Cement and Concrete Composites, 18 (1996) 67-76.
[100] L. Huang, L. Yu, H. Zhang, Z. Yang, Composition and microstructure of 50-year lightweight aggregate concrete (LWAC) from Nanjing Yangtze River bridge (NYRB), Construction and Building Materials, 216 (2019) 390-404.
[101] M.-H. Zhang, O. Gjørv, Backscattered electron imaging studies on the interfacial zone between high strength lightweight aggregate and cement paste, Advances in Cement Research, 2 (1989) 141-146.
[102] M.D. Andersen, H.J. Jakobsen, J. Skibsted, Characterization of white Portland cement hydration and the C-S-H structure in the presence of sodium aluminate by 27Al and 29Si MAS NMR spectroscopy, Cement and Concrete Research, 34 (2004) 857-868.
[103] Z. Dai, T.T. Tran, J. Skibsted, H. Jennings, Aluminum incorporation in the C-S-H phase of white Portland cement-metakaolin blends studied by 27
Al and 29
Si MAS NMR Spectroscopy, Journal of the American Ceramic Society, 97 (2014) 2662-2671.
[104] P. Shen, L. Lu, Y. He, F. Wang, S. Hu, The effect of curing regimes on the mechanical properties, nano-mechanical properties and microstructure of ultra-high performance concrete, Cement and Concrete Research, 118 (2019) 1-13.
[105] L. Wang, H.Q. Yang, S.H. Zhou, E. Chen, S.W. Tang, Hydration, mechanical property and C-S-H structure of early-strength low-heat cement-based materials, Materials Letters, 217 (2018) 151-154.
[106] C. Liu, L. Yang, F. Wang, S. Hu, Enhance the durability of heat-cured mortars by internal curing and pozzolanic activity of lightweight fine aggregates, Construction and Building Materials, 270 (2021) 121439.
[107] H. Zhang, L. Huang, L. Yu, Z. Yang, Macromechanical properties and ITZ of lightweight aggregate concrete from the deck of Nanjing Yangtze River bridge after 50 Years, Journal of Materials in Civil Engineering Structures, 32 (2020) 05020005.
[108] G. Constantinides, F.-J. Ulm, The nanogranular nature of C–S–H, Journal of the Mechanics and Physics of Solids, 55 (2007) 64-90.
[109] C. Hu, Z. Li, A review on the mechanical properties of cement-based materials measured by nanoindentation, Construction and Building Materials, 90 (2015) 80-90.
[110] M. Vandamme, F.-J. Ulm, P. Fonollosa, Nanogranular packing of C–S–H at substochiometric conditions, Cement and Concrete Research, 40 (2010) 14-26.
[111] S. Zhao, W. Sun, Nano-mechanical behavior of a green ultra-high performance concrete, Construction and Building Materials, 63 (2014) 150-160.
[112] S. Cheng, Z. Shui, T. Sun, Y. Huang, K. Liu, Effects of seawater and supplementary cementitious materials on the durability and microstructure of lightweight aggregate concrete, Construction and Building Materials, 190 (2018) 1081-1090.
[113] L. Kong, B. Zhang, Y. Ge, J. Yuan, Effect of ceramsite structure on microstructure of interfacial zone and durability of combined aggregate concrete, Journal of Wuhan University of Technology-Mater. Sci. Ed., 24 (2009) 145-149.
[114] K.K. Aligizaki, Pore structure of cement-based materials: testing, interpretation and requirements, CRC Press, London, 2006.
[115] Y. Liu, Y. Wei, Effect of calcined bauxite powder or aggregate on the shrinkage properties of UHPC, Cement and Concrete Composites, 118 (2021) 103967.
[116] P.K. Mehta, P.J.M. Monteiro, Concrete: Microstructure, Properties and Materials, McGraw-Hill, Third edition, USA, New York, (2006).
[117] M.-H. Zhang, O.E. Gjørv, Mechanical properties of high-strength lightweight concrete, ACI Material Journal, 88 (1991) 240-247.
[118] S. Ghourchian, M. Wyrzykowski, P. Lura, M. Shekarchi, B. Ahmadi, An investigation on the use of zeolite aggregates for internal curing of concrete, Construction and Building Materials, 40 (2013) 135-144.
[119] A.J. Tenza-Abril, D. Benavente, C. Pla, F. Baeza-Brotons, J. Valdes-Abellan, A.M. Solak, Statistical and experimental study for determining the influence of the segregation phenomenon on physical and mechanical properties of lightweight concrete, Construction and Building Materials, 238 (2020) 117642.
[120] R. Yu, F. Zhou, T. Yin, Z. Wang, M. Ding, Z. Liu, Y. Leng, X. Gao, Z. Shui, Uncovering the approach to develop

ultra-high performance concrete (UHPC) with dense meso-structure based on rheological point of view: Experiments and modeling, Construction and Building Materials, 271 (2021) 121500.
[121] N. Van Tuan, G. Ye, K. van Breugel, O. Copuroglu, Hydration and microstructure of ultra high performance concrete incorporating rice husk ash, Cement and Concrete Research, 41 (2011) 1104-1111.
[122] R. Yu, P. Spiesz, H.J.H. Brouwers, Mix design and properties assessment of Ultra-High Performance Fibre Reinforced Concrete (UHPFRC), Cement and Concrete Research, 56 (2014) 29-39.
[123] X. Liu, K.S. Chia, M.-H. Zhang, Water absorption, permeability, and resistance to chloride-ion penetration of lightweight aggregate concrete, Construction and Building Materials, 25 (2011) 335-343.
[124] X. Liu, M.H. Zhang, Permeability of high-performance concrete incorporating presoaked lightweight aggregates for internal curing, Magazine of Concrete Research, 62 (2010) 79-89.
[125] S. Zhutovsky, K. Kovler, Effect of internal curing on durability-related properties of high performance concrete, Cement and Concrete Research, 42 (2012) 20-26.
[126] M.-H. Zhang, V.M. Malhotra, High-performance concrete incorporating rice husk ash as a supplementary cementing material, ACI Materials Journal, 93 (1996) 629-636.
[127] T. Xie, C. Fang, M.S. Mohamad Ali, P. Visintin, Characterizations of autogenous and drying shrinkage of ultra-high performance concrete (UHPC): An experimental study, Cement and Concrete Composites, 91 (2018) 156-173.
[128] A.M. Soliman, M.L. Nehdi, Effects of shrinkage reducing admixture and wollastonite microfiber on early-age behavior of ultra-high performance concrete, Cement and Concrete Composites, 46 (2014) 81-89.
[129] P. Lura, M. Wyrzykowski, C. Tang, E. Lehmann, Internal curing with lightweight aggregate produced from biomass-derived waste, Cement and Concrete Research, 59 (2014) 24-33.
[130] P. Shen, J.-X. Lu, H. Zheng, L. Lu, F. Wang, Y. He, S. Hu, Expansive ultra-high performance concrete for concrete-filled steel tube applications, Cement and Concrete Composites, 114 (2020).
[131] K. Liu, R. Yu, Z. Shui, X. Li, C. Guo, B. Yu, S. Wu, Optimization of autogenous shrinkage and microstructure for Ultra-High Performance Concrete (UHPC) based on appropriate application of porous pumice, Construction and Building Materials, 214 (2019) 369-381.
[132] Y. Sun, R. Yu, Z. Shui, X. Wang, D. Qian, B. Rao, J. Huang, Y. He, Understanding the porous aggregates carrier effect on reducing autogenous shrinkage of Ultra-High Performance Concrete (UHPC) based on response surface method, Construction and Building Materials, 222 (2019) 130-141.
[133] M. Thomas, The effect of supplementary cementing materials on alkali-silica reaction: A review, Cement and Concrete Research, 41 (2011) 1224-1231.
[134] Y. Liu, Y. Wei, Internal curing by porous calcined bauxite aggregate in ultra high-performance concrete, Journal of Materials in Civil Engineering, 33 (2021) 04020497.